

1 SEARCH FOR PRODUCTION OF A HIGGS BOSON AND A SINGLE TOP  
2 QUARK IN MULTILEPTON FINAL STATES IN  $pp$  COLLISIONS AT  $\sqrt{s} = 13$   
3 TeV.

4 by

5 Jose Andres Monroy MontaÑez

6 A DISSERTATION

7 Presented to the Faculty of

8 The Graduate College at the University of Nebraska

In Partial Fulfilment of Requirements

10 For the Degree of Doctor of Philosophy

11 Major: Physics and Astronomy

12 Under the Supervision of Kenneth Bloom and Aaron Dominguez

13 Lincoln, Nebraska

14 July, 2018

15 SEARCH FOR PRODUCTION OF A HIGGS BOSON AND A SINGLE TOP  
16 QUARK IN MULTILEPTON FINAL STATES IN pp COLLISIONS AT  $\sqrt{s} = 13$   
17 TeV.

18 Jose Andres Monroy Montañez, Ph.D.

19 University of Nebraska, 2018

20 Adviser: Kenneth Bloom and Aaron Dominguez

# <sup>21</sup> Table of Contents

<sup>22</sup>	<b>Table of Contents</b>	<b>iii</b>
<sup>23</sup>	<b>List of Figures</b>	<b>vi</b>
<sup>24</sup>	<b>List of Tables</b>	<b>viii</b>
<sup>25</sup>	<b>1 INTRODUCTION</b>	<b>1</b>
<sup>26</sup>	<b>2 Theoretical approach</b>	<b>2</b>
<sup>27</sup>	2.1 Introduction . . . . .	2
<sup>28</sup>	2.2 Standard model of particle physics . . . . .	4
<sup>29</sup>	2.2.1 Fermions . . . . .	6
<sup>30</sup>	2.2.1.1 Leptons . . . . .	7
<sup>31</sup>	2.2.1.2 Quarks . . . . .	10
<sup>32</sup>	2.2.2 Fundamental interactions . . . . .	13
<sup>33</sup>	2.2.3 Gauge Bosons . . . . .	19
<sup>34</sup>	2.3 Electroweak unification and the Higgs mechanism . . . . .	20
<sup>35</sup>	2.3.1 Spontaneous symmetry breaking . . . . .	28
<sup>36</sup>	2.3.2 Higgs mechanism . . . . .	32
<sup>37</sup>	2.3.3 Masses of the gauge bosons . . . . .	34

38	2.3.4	Masses of the fermions . . . . .	35
39	2.3.5	The Higgs field . . . . .	36
40	2.3.6	Higgs boson production mechanisms at LHC. . . . .	37
41	2.3.7	Higgs decay channels . . . . .	40
42	2.4	Associated Production of Higgs Boson and Single Top Quark. . . . .	41
43	2.5	The CP-mixing phase . . . . .	41
44	<b>3</b>	<b>The CMS experiment at the LHC</b>	<b>42</b>
45	3.1	The LHC . . . . .	43
46	3.2	The CMS experiment . . . . .	46
47	<b>4</b>	<b>Search for production of a Higgs boson and a single top quark in multilepton final states in pp collisions at <math>\sqrt{s} = 13</math> TeV</b>	<b>48</b>
49	4.1	Introduction . . . . .	48
50	4.2	Data and MC Samples . . . . .	50
51	4.2.1	Full 2016 dataset and MC samples . . . . .	50
52	4.2.2	Triggers . . . . .	53
53	4.2.2.1	Trigger efficiency scale factors . . . . .	53
54	4.3	Object Identification and event selection . . . . .	54
55	4.3.1	Jets and $b$ tagging . . . . .	54
56	4.3.2	Lepton selection . . . . .	55
57	4.3.3	Lepton selection efficiency . . . . .	56
58	4.4	Background predictions . . . . .	57
59	4.5	Signal discrimination . . . . .	58
60	4.5.1	Classifiers response . . . . .	62
61	4.6	Additional discriminating variables . . . . .	65

62	<b>5 The CMS forward pixel detector</b>	<b>68</b>
63	5.0.1 The phase 1 FPix upgrade . . . . .	68
64	5.0.2 FPix module production line . . . . .	68
65	5.0.3 The Gluing stage . . . . .	68
66	5.0.4 The Encapsulation stage . . . . .	68
67	5.0.5 The FPix module production yields . . . . .	68
68	<b>Bibliography</b>	<b>68</b>
69	<b>References</b>	<b>69</b>

# <sup>70</sup> List of Figures

71	1.1	$^{14}N$ neutron capture in a PECVD polymerized pyridine film. The Q-value 72 of this reaction is 626 keV. Taken from [22] . . . . .	1
73	2.1	Standard model of particle physics. . . . .	5
74	2.2	WI transformations between quarks . . . . .	12
75	2.3	Fundamental interactions in nature. . . . .	13
76	2.4	SM interactions diagrams . . . . .	15
77	2.5	Neutral current processes . . . . .	21
78	2.6	Spontaneous symmetry breaking mechanism . . . . .	28
79	2.7	SSB Potential form . . . . .	29
80	2.8	Potential for complex scalar field . . . . .	30
81	2.9	SSB mechanism for complex scalar field . . . . .	31
82	2.10	Higgs production mechanism Feynman diagrams . . . . .	38
83	2.11	Higgs production cross section and decay branching ratios . . . . .	39
84	3.1	ref. C.Lefevre, “The CERN accelerator complex,” (2008). CERN-DI- 85 0812015. . . . .	44

86	3.2	ref. J.-L. Caron , “Layout of the LEP tunnel including future LHC in-	
87		frastructures.. L’ensemble du tunnel LEP avec les futures infrastructures	
88		LHC.”, <a href="https://cds.cern.ch/record/841542">https://cds.cern.ch/record/841542</a> (Nov, 1993). AC Collection.	
89		Legacy of AC. Pictures from 1992 to 2002.. . . . .	45
90	3.3	ref. ACTeam, “Diagram of an LHC dipole magnet. Schéma d’un aimant	
91		dipôle du LHC,” (1999). CERN-DI-9906025. . . . .	46
92	3.4	ref: CMS Collaboration, “Detector Drawings”, CMS-PHO-GEN-2012-002,	
93		<a href="http://cds.cern.ch/record/1433717">http://cds.cern.ch/record/1433717</a> , 2012. . . . .	47
94	4.1	The two leading-order diagrams of $tHq$ production. . . . .	49
95	4.2	Input variables to the BDT for signal discrimination normalized. . . . .	59
96	4.3	Input variables to the BDT for signal discrimination not normalized. . .	61
97	4.4	BDT inputs as seen by TMVA against $t\bar{t}$ . . . . .	62
98	4.5	BDT inputs as seen by TMVA against $t\bar{t}V$ . . . . .	63
99	4.6	Correlation matrices for the input variables in the TMVA. . . . .	64
100	4.7	MVA classifiers performance. . . . .	64
101	4.8	Additional discriminating variables distributions. . . . .	66

# <sup>102</sup> List of Tables

103	2.1	Fermions of the SM.	7
104	2.2	Leptons properties.	9
105	2.3	Quarks properties.	10
106	2.4	Fermion weak isospin and weak hypercharge multiplets.	11
107	2.5	Fundamental interactions features.	16
108	2.6	SM gauge bosons.	20
109	2.7	Higgs boson properties.	36
110	2.8	Branching ratios for a SM Higgs boson with $m_H = 125$ GeV/c <sup>2</sup> .	40
111	4.1	Signal samples and their cross section and branching fraction.	50
112	4.2	$\kappa_V$ and $\kappa_t$ combinations.	51
113	4.3	List of background samples used in this analysis (CMSSW 80X).	52
114	4.4	Leading-order $t\bar{t}W$ and $t\bar{t}Z$ samples used in the signal BDT training.	52
115	4.5	Table of high-level triggers that we consider in the analysis.	53
116	4.6	Trigger efficiency scale factors and associated uncertainties.	54
117	4.7	Requirements on each of the three muon selections.	55
118	4.8	Criteria for each of the three electron selections.	56
119	4.9	MVA input discriminating variables	60
120	4.10	TMVA input variables ranking for BDTA_GRAD method	65

121	4.11 TMVA configuration used in the BDT training. . . . .	65
122	4.12 ROC-integral for all the testing cases. . . . .	67

<sup>123</sup> Chapter 1

<sup>124</sup> INTRODUCTION

**Figure 1.1:**  $^{14}N$  neutron capture in a PECVD polymerized pyridine film. The Q-value of this reaction is 626 keV. Taken from [22]

<sub>125</sub> **Chapter 2**

<sub>126</sub> **Theoretical approach**

<sub>127</sub> **2.1 Introduction**

<sub>128</sub> The physical description of the universe is a challenge that physicists have faced by  
<sub>129</sub> making theories that refine existing principles and proposing new ones in an attempt  
<sub>130</sub> to embrace emerging facts and phenomena. By early 1800's, there were separate  
<sub>131</sub> theories describing electric and magnetic phenomena, gravitational force and light.  
<sub>132</sub> The invention of the electric battery by Alessandro Volta in 1800, the discovery  
<sub>133</sub> of the magnetic effects of the electric current by Oersted and Ampere (1820), and  
<sub>134</sub> the generation of electric current using changing magnetic fields by Faraday (1831)  
<sub>135</sub> represent the first steps in the way to create a unified theory of electromagnetism [1].

<sub>136</sub> The unification was carried out by James Clerk Maxwell who was able to merge  
<sub>137</sub> electricity and magnetism in a set of 20 equations known as "general equations of the  
<sub>138</sub> electromagnetic field," relating the observables that describe the experimental laws of  
<sub>139</sub> the electromagnetism. By combining these equations, Maxwell found a wave equation  
<sub>140</sub> and propose the existence of the "electromagnetic waves." The predicted propagation  
<sub>141</sub> speed of the electromagnetic waves turned out to be the same as the speed of light,

142 therefore, the natural conclusion was that light is an electromagnetic wave [4]. By  
 143 1900, waves were considered a perturbation of a material medium which in the case  
 144 of the electromagnetic waves was identified as the “*Luminiferous Ether*”. 

145 By 1900, Max Planck came out with the idea that radiation is quantized [5] and Albert  
 146 Einstein in 1905 made use of that hypothesis to propose the existence of the light  
 147 quantum, the “*photon*”, in order to explain the photoelectric effect [6]. The well-  
 148 known quantum revolution in physics started and the idea of particle-wave duality  
 149 of photons as a natural behavior was developed and later extended to electrons and  
 150 to all kind of particles in nature. The development of a quantum theory allowed  
 151 to predict a set of non-common sense effects like the quantum tunneling and quan-  
 152 tum entanglement, however, quantum theory was separated from the recently unified  
 153 electromagnetism.

154 In 1905, Einstein also published two more papers; one aimed to describe his statistical  
 155 molecular theory of liquids and how it can be used to describe Brownian motion  [7].

156 At that time the existence of the atoms and molecules were not fully demonstrated  
 157 but Einstein’s theory provided an explanation  as well as predictions based on the  
 158 their existence. Jean Perrin in 1908 conducted experiments that confirmed Einstein’s  
 159 predictions.  other paper described the relationship between space and time [8],

160 unifying the notion of space and time into one entity known as “*spacetime*” that treats  
 161 space and time at the same level and then discards the absoluteness of time. The  
 162 new theory known as special relativity, supersedes the Galilean relativity principle  
 163 and postulates exceptional effects like the time dilation, length contraction and mass-  
 164 energy equivalence through the most famous formula in physics  [9]

$$E = mc^2. \quad (2.1)$$

165 Generalization of the special relativity was presented in 1916 and includes a gener-  
 166 alization of Newton’s law of universal gravitation, becoming a unified description of  
 167 gravity as a geometric property of space and time. Einstein’s predictions include the  
 168 existence of black holes and the recently observed “*gravitational waves*” [10].

169 At the end of 1940s Julian Schwinger [11] and Richard P. Feynman [12], based in  
 170 the work of Sin-Itiro Tomonaga [13], developed an electromagnetic theory consistent  
 171 with special relativity and quantum mechanics that describes how matter and light  
 172 interact; so-called “quantum eletrodynamics” (QED)  born.

173 QED has become the guide in the development of theories that describe the universe.  
 174 It was the first example of a quantum field theory  (QFT), which is the theoretical  
 175 framework for building quantum mechanical models that describes particles and their  
 176 interactions. QFT is composed of a set of mathematical tools that combines classical  
 177 fields, special relativity, and quantum mechanics while keeping the quantum point  
 178 particles and locality ideas. This chapter gives an overview of the SM  starting with  
 179 the SM particle content, followed by a description of the electroweak interaction,  
 180 the Higgs boson and the associated production of Higgs boson and a single top quark  
 181 ( $tH$ ). The description contained in this chapter is based on references ?? unless explicit  
 182 reference is provided.

## 183 2.2 Standard model of particle physics

184 Particle physics at the fundamental level is modeled in terms of a collection of in-  
 185 teracting particles and fields in a theory known as the “standard model of particle  
 186 physics (SM)”<sup>1</sup>.

---

<sup>1</sup> The formal and complete treatment of the SM is out of the scope of this document, however a plenty of textbooks describing it at several levels are available in the literature. The treatment in “An Introduction To Quantum Field Theory (Frontiers in Physics)” by Michael E. Peskin

The full picture of the SM is composed of three fields<sup>2</sup>, whose excitations are interpreted as particles called mediators or force-carriers; a set of fields, whose excitations are interpreted as elementary particles, interacting through the exchange of those mediators and a field that give the mass to elementary particles. Figure 2.1 shows an scheme of the SM particles organization. In addition to the particles in the scheme, their corresponding anti-particles, with opposite quantum numbers, are also part of the picture. Some particles are their own anti-particles, like photon or Higgs, or anti-particle is already listed like in the  $W^+$  and  $W^-$  case.

# Standard Model of Elementary Particles

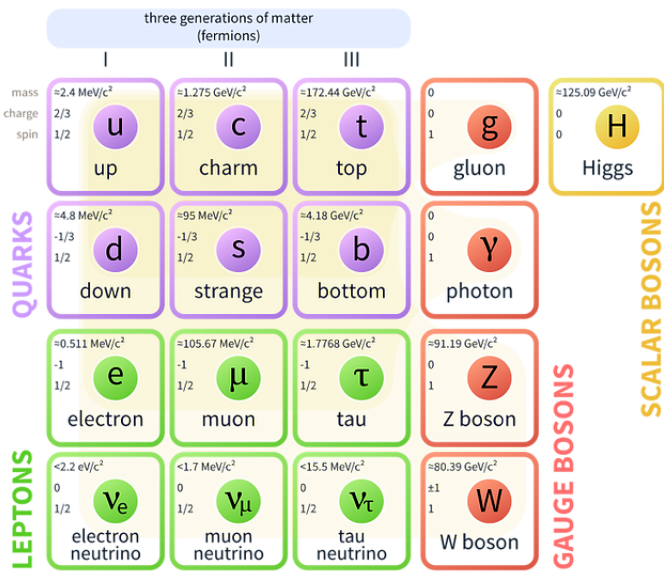


**Figure 2.1:** Schematic representation of the Standard model of particle physics. SM is a theoretical model intended to describe three of the four fundamental forces of the universe in terms of a set of particles and their interactions. [18].

195 The mathematical formulation of the SM is based on group theory and the use of  
 196 Noether's theorem [17] which states that for a physical system modeled by a La-  
 197 grangian that is invariant under a group of transformations a conservation law is

and Dan V. Schroeder is quite comprehensive and detailed.

<sup>2</sup> Note that gravitational field is not included in the standard model formulation

198 expected. For instance, a system described by a time-independent Lagrangian is  
 199 invariant (symmetric) under time changes (transformations) with the total energy  
 200 conservation law as the expected conservation law. In QED, the  operator is the  
 201 generator of the U(1) symmetry which according to the Noether's theorem means  
 202 that there is a conserved charge; this conserved charge is the electric charge and thus  
 203 the law conservation of electric charge is established.

204 In the SM, the symmetry group  $SU(3)_C \otimes SU(2)_L \otimes U(1)_Y$  describes three of the  
 205 four fundamental interactions in nature(see section 2.2.2): strong interaction(SI),  
 206 weak interaction(WI) and electromagnetic interactions (EI) in terms of symmetries  
 207 associated to physical quantities:

- 208     • Strong:  $SU(3)_C$  associated to color charge
- 209     • Weak:  $SU(2)_L$  associated to weak isospin and chirality
- 210     • Electromagnetic:  $U(1)_Y$  associated to weak hypercharge and electric charge

211 It will be shown that the electromagnetic and weak interactions are combined in  
 212 the so-called electroweak interaction where chirality, hypercharge, weak isospin and  
 213 electric charge are the central concepts.

### 214 2.2.1 Fermions

215 The basic constituents of the ordinary matter at the lowest level, which form the  
 216 set of elementary particles in the SM formulation, are quarks and leptons. All of  
 217 them have spin 1/2, therefore they are classified as fermions since they obey Fermi-  
 218 Dirac statistics. In both cases, they come in six “flavors” and are organized in three  
 219 generations, or families, as shown in table 2.1.

220 There is a mass hierarchy between generations where the higher generation particles  
 221 decays to the lower one which can explain why the ordinary matter is made of particles  
 222 in the first generation. In the SM, neutrinos are modeled as massless particles so they  
 223 are not subject to this mass hierarchy; however, today it is known that neutrinos are  
 224 massive so the hierarchy could be restated. The reason behind this mass hierarchy is  
 225 one of the most important open questions in particle physics, and it becomes more  
 226 puzzling when noticing that the mass difference between first and second generation  
 227 fermions is small compared to the mass difference with respect to the third generation.  
 228 Usually, the second and third generation fermions are produced in high energy pro-  
 229 cesses, like the ones recreated in the particle accelerators.

Generation				
	Type	1st	2nd	3rd
Leptons	Charged	Electron (e)	Moun( $\mu$ )	Tau ( $\tau$ )
	Neutral	Electron neutrino ( $\nu_e$ )	Muon neutrino ( $\nu_\mu$ )	Tau neutrino ( $\nu_\tau$ )
Quarks	Up-type	Up (u)	Charm (c)	Top (t)
	Down-type	Down (d)	Starnge (s)	Bottom (b)

**Table 2.1:** Fermions of the SM. Quarks and leptons comes in six flavors each and are organized in three generations or families composed of two pairs of closely related particles. The close relationship is motivated by the fact that WI between leptons is limited to the members of the same generation. Generations differs by mass in a way that have been interpreted as a masss hierarchy.

230

### 231 2.2.1.1 Leptons

232 A lepton is an elementary particle that is not subject to the SI. As seen in table 2.1,  
 233 there are two types of leptons, the charged ones (electron, muon and tau) and the  
 234 neutral ones (the three neutrinos). The electric charge (Q) is the property that gives  
 235 leptons the ability to participate in the EI. From the classical point of view, Q plays  
 236 a central role determining, among others, the strength of the electric field through

237 which the electromagnetic force is exerted. It is clear that neutrinos are not affected  
 238 by EI because they don't carry electric charge.

239 Another feature of the leptons that is fundamental in the mathematical description  
 240 of the SM is the chirality, which is closely related to spin and helicity. Helicity  
 241 define the handedness of a particle by relating its spin and momentum such that  
 242 if they are parallel then the particle is right-handed; if spin and momentum are  
 243 antiparallel the particle is said to be left-handed. The study of parity conservation  
 244 (or violation) in  $\beta$ -decay have shown that only left-handed electrons/neutrinos or  
 245 right-handed positrons/anti-neutrinos are created [19]; the inclusion of that feature  
 246 in the theory was reached by using projection operators for helicity, however, helicity is  
 247 frame dependent for massive particles which makes it not Lorentz invariant and then  
 248 another related attribute has to be used: *chirality*. Chirality is a purely quantum  
 249 attribute which makes it not so easy to describe in graphical terms but it defines  
 250 how the wave function of a particle transforms under certain rotations. As with  
 251 helicity, there are two chiral states, left-handed chiral (L) and right-handed chiral  
 252 (R). In the highly relativistic limit where  $E \approx p \gg m$  helicity and chirality converge,  
 253 becoming exactly the same for massless particles. In the following when referring  
 254 to left-handed (right-handed) it means left-handed chiral (right-handed chiral). The  
 255 fundamental fact about chirality is that while EI and SI are not sensitive to chirality,  
 256 in WI left-handed and right-handed fermions are treated asymmetrically, such that  
 257 only left handed fermions and right-handed anti-fermions are allowed to couple to WI  
 258 mediators, which is a violation of parity. The way to translate this statement in a  
 259 formal mathematical formulation is based on the isospin symmetry group  $SU(2)_L$ .  
 260 Each generation of leptons is seen as a weak isospin doublet.<sup>3</sup> The left-handed charged

---

<sup>3</sup> The weak isospin is an analogy of the isospin symmetry in strong interaction where neutron and proton are affected equally by strong force but differ in its charge.

261 lepton and its associated left-handed neutrino are arranged in doublets of weak isospin  
 262  $T=1/2$  while their right-handed partners are singlets:

$$\begin{pmatrix} \nu_l \\ l \end{pmatrix}_L, l_R := \begin{pmatrix} \nu_e \\ e \end{pmatrix}_L, \begin{pmatrix} \nu_\mu \\ \mu \end{pmatrix}_L, \begin{pmatrix} \nu_\tau \\ \tau \end{pmatrix}_L, e_R, \mu_R, \tau_R, \nu_{eR}, \nu_{\mu R}, \nu_{\tau R} \quad (2.2)$$

263 The isospin third component refers to the eigenvalues of the weak isospin operator  
 264 which for doublets is  $T_3 = \pm 1/2$ , while for singlets it is  $T_3 = 0$ . The physical meaning  
 265 of this doublet-singlet arrangement falls in that the WI couples the two particles in  
 266 the doublet by exchanging the interaction mediator while the singlet member is not  
 267 involved in WI. The main properties of the leptons are summarized in table 2.2.  
 268 Altough all three flavor neutrinos have been observed, their masses remain unknown  
 269 and only some estimations have been made [20]. The main reason is that the fla-  
 270 vor eigenstates are not the same as the mass eigenstates which imply that when a  
 271 neutrino is created its mass state is a linear combination of the three mass eigen-  
 272 states and experiments can only probe the squared difference of the masses. The  
 273 Pontecorvo-Maki-Nakagawa-Sakata (PMNS) mixing matrix encode the relationship  
 274 between flavor and mass eigenstates.

Lepton	Q(e)	$T_3$	$L_e$	$L_\mu$	$L_\tau$	Mass (MeV/c <sup>2</sup> )	Lifetime (s)
Electron (e)	-1	-1/2	1	0	0	0.5109989461(31)	Stable
Electron neutrino( $\nu_e$ )	0	1/2	1	0	0	Unknown	Unknown
Muon ( $\mu$ )	-1	-1/2	0	1	0	105.6583745(24)	$2.1969811(22) \times 10^{-6}$
Muon neutrino ( $\nu_\mu$ )	0	1/2	0	1	0	Unknown	Unknown
Tau ( $\tau$ )	-1	-1/2	0	0	1	1776.86(12)	$290.3(5) \times 10^{-15}$
Tau neutrino ( $\tau_\mu$ )	0	1/2	0	0	1	Unknown	Unknown

**Table 2.2:** Leptons properties [21]. Q: electric charge,  $T_3$ : weak isospin. Only left-handed leptons and right-handed anti-leptons participate in the WI. Anti-particles with inverted  $T_3$ , Q and lepton number complete the leptons set but are not listed. Right-handed leptons and left-handed anti-leptons, neither listed, form weak isospin singlets with  $T_3 = 0$  and do not take part in the weak interaction.

276 **2.2.1.2 Quarks**

277 Quarks are the basic constituents of protons, neutrons and other non-elementary  
 278 particles. The way quarks join to form bound states, called “hadrons”, is through  
 279 the SI. Quarks are affected by all the fundamental interactions which means that  
 280 they carry all the four types of charges: color, electric charge, weak isospin and mass.  
 281 Table 2.3 summarizes the features of quarks, among which the most particular is  
 282 their fractional electric charge. Note that fractional charge is not a problem, given  
 283 that quarks are not found isolated, but serves to explain how composed particles are  
 284 formed out of two or more valence quarks<sup>4</sup>.

Flavor	$Q(e)$	$I_3$	$T_3$	B	C	S	T	$B'$	Y	Color	Mass (MeV/c <sup>2</sup> )
Up (u)	2/3	1/2	1/2	1/3	0	0	0	0	1/3	r,b,g	$2.2^{+0.6}_{-0.4}$
Charm (c)	2/3	0	1/2	1/3	1	0	0	0	4/3	r,b,g	$1.28 \pm 0.03 \times 10^3$
Top(t)	2/3	0	1/2	1/3	0	0	1	0	4/3	r,b,g	$173.1 \pm 0.6 \times 10^3$
Down(d)	-1/3	-1/2	-1/2	1/3	0	0	0	0	1/3	r,b,g	$4.7^{+0.5}_{-0.4}$
Strange(s)	-1/3	0	-1/2	1/3	0	-1	0	0	-2/3	r,b,g	$96^{+8}_{-4}$
Bottom(b)	-1/3	0	-1/2	1/3	0	0	0	-1	-2/3	r,b,g	$4.18^{+0.04}_{-0.03} \times 10^3$

**Table 2.3:** Quarks properties [21]. Q: electric charge,  $I_3$ : isospin,  $T_3$ : weak isospin, B: baryon number, C: charmness, S: strangeness, T: topness,  $B'$ : bottomness, Y: hypercharge. Anti-quarks posses the same mass and spin as quarks but all charges (color, flavor numbers) have opposite sign.

285

286 Color charge is the responsible for the SI between quarks and is the symmetry  
 287 ( $SU(3)_C$ ) that defines the formalism to describe SI. There are three colors: red (r),  
 288 blue(b) and green(g) and their corresponding three anti-colors; thus each quark carries  
 289 one color unit while anti-quarks carries one anti-color unit. As said above, quarks are  
 290 not allowed to be isolated due to the color confinement effect, therefore their features  
 291 have been studied indirectly by observing their bound states created when:

<sup>4</sup> Hadrons can contain an indefinite number of virtual quarks and gluons, known as the quark and gluon sea, but only the valence quarks determine hadrons' quantum numbers.

- 292     • one quark with a color charge is attracted by an anti-quark with the correspond-  
 293         ing anti-color charge forming a colorless particle called a “meson.”
- 294     • three quarks (anti-quarks) with different color (anti-color) charges are attracted  
 295         among them forming a colorless particle called a “baryon(anti-baryon).”
- 296     In the first version of the quark model (1964), M. Gell-Mann [22] and G. Zweig [23,24]  
 297     developed a consistent way to classify hadrons according to their properties. Only  
 298     three quarks (u, d, s) were involved in a scheme in which all baryons have baryon  
 299     number  $B=1$  and therefore quarks have  $B=1/3$ ; non-baryons have  $B=0$ . The scheme  
 300     organize baryons in a two-dimensional space ( $I_3$  - Y); Y (hypercharge) and  $I_3$  (isospin)  
 301     are quantum numbers related by the Gell-Mann-Nishijima formula [25,26]:

$$Q = I_3 + \frac{Y}{2} \quad (2.3)$$

302     where  $Y = B + S + C + T + B'$  are the quantum numbers listed in table 2.3. Baryon  
 303     number is conserved in SI and EI which means that single quarks cannot be created  
 304     but in pairs  $q - \bar{q}$ .  
 305     Similar to leptons, there are six quark flavors organized in three generations (see table  
 306     2.1) and follow a mass hierarchy which again implies that higher generations decay  
 307     to first generation quarks.

	Quarks			$T_3$	$Y_W$	Leptons			$T_3$	$Y_W$
Doublets	$(\begin{smallmatrix} u \\ d' \end{smallmatrix})_L$	$(\begin{smallmatrix} c \\ s' \end{smallmatrix})_L$	$(\begin{smallmatrix} t \\ b' \end{smallmatrix})_L$	$(\begin{smallmatrix} 1/2 \\ -1/2 \end{smallmatrix})$	1/3	$(\begin{smallmatrix} \nu_e \\ e \end{smallmatrix})_L$	$(\begin{smallmatrix} \nu_\mu \\ \mu \end{smallmatrix})_L$	$(\begin{smallmatrix} \nu_\tau \\ \tau \end{smallmatrix})_L$	$(\begin{smallmatrix} 1/2 \\ -1/2 \end{smallmatrix})$	-1
Singlets	$u_R$	$c_R$	$t_R$	0	4/3	$\nu_{eR}$	$\nu_{\mu R}$	$\nu_{\tau R}$	0	-2

**Table 2.4:** Fermion weak isospin and weak hypercharge multiplets. Weak hypercharge is calculated through the Gell-Mann-Nishijima formula 2.3 but using the weak isospin and charge for quarks.

309 Isospin doublets of quarks are also defined (see table 2.4) and as for neutrinos, the  
 310 mass eigenstates are not the same as the WI eigenstates which means that members of  
 311 different quark generations are connected by the WI mediator; thus, up-type quarks  
 312 are coupled not to down-type quarks directly but to a superposition of down-type  
 313 quarks ( $q'_d$ ) via WI according to:

$$314 \quad q'_d = V_{CKM} q_d$$

$$\begin{pmatrix} d' \\ s' \\ b' \end{pmatrix} = \begin{pmatrix} V_{ud} & V_{us} & V_{ub} \\ V_{cd} & V_{cs} & V_{cb} \\ V_{td} & V_{ts} & V_{tb} \end{pmatrix} \begin{pmatrix} d \\ s \\ b \end{pmatrix} \quad (2.4)$$

315 where  $V_{CKM}$  is known as Cabibbo-Kobayashi-Maskawa (CKM) mixing matrix [27,28].

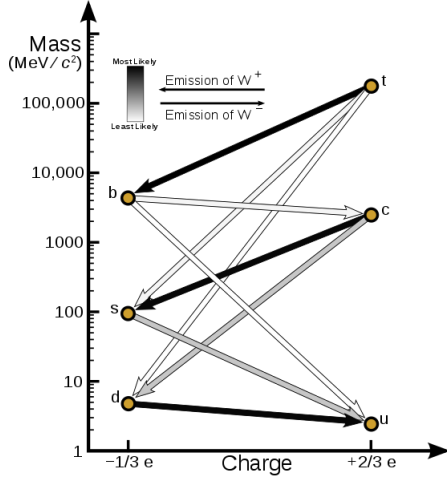


**Figure 2.2:** Transformations between quarks through WI. Higher generations quarks decay to first generation quarks by emitting a W boson. The arrow color indicates the likelihood of the transition according to the grey scale in the top left side which represent the CKM matrix parameters [29].

316 The weak decays of quarks are represented in the diagram of figure 2.2; again the CKM  
 317 matrix plays a central role since it contains the probabilities for the different quark  
 318 decay channels, in particular, note that quark decays are greatly favored between

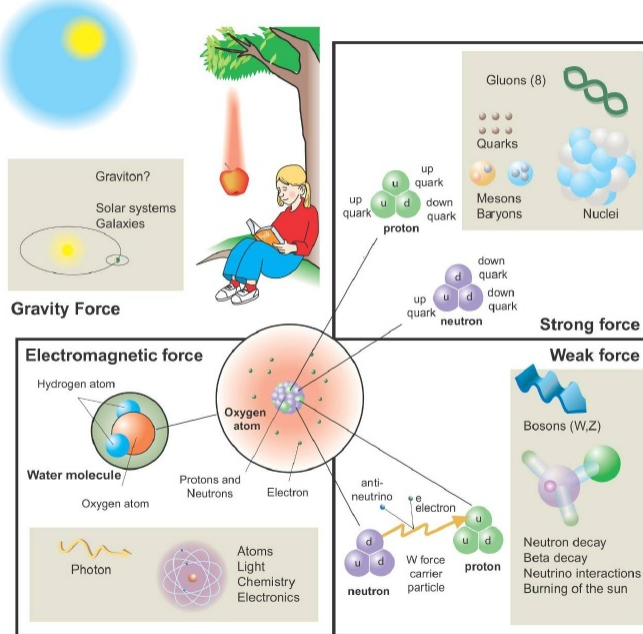
319 generation members.

320 CKM matrix is a  $3 \times 3$  unitary matrix parametrized by three mixing angles and the  
 321 *CP-mixing phase*; the latter is the parameter responsible for the CP-violation in the  
 322 SM. The fact that the b quark decays almost all the times to a top quark is exploited  
 323 in this thesis when making the selection of the signal events by requiring the presence  
 324 of a jet tagged as a jet coming from a b quark in the final state. The effect of the  
 325 *CP-mixing phase* on the cross section of associated production of Higgs boson and a  
 326 single top process is also explored in this thesis.

### 327 2.2.2 Fundamental interactions

#### Fundamental interactions.

Illustration: Typoform



Summer School KPI 15 August 2009

**Figure 2.3:** Fundamental interactions in nature. Despite the many manifestations of forces in nature, we can track all of them back to one of the fundamental interactions. The most common forces are gravity and electromagnetic given that all of us are subject and experience them in everyday life.

328 Even though there are many manifestations of force in nature, like the ones represented  
 329 in figure 2.3, we can classify all of them into one of four fundamental interactions:  
 330

331 • *Electromagnetic interaction (EI)* affect particles that are “electrically charged,”  
 332 like electrons and protons. It is described by QED combining quantum mechanics,  
 333 special relativity and electromagnetism in order to explain how particles  
 334 with electric charge interact through the exchange of photons, therefore, one  
 335 says that “Electromagnetic Force” is mediated by “photons”. Figure 2.4a) shows  
 336 a graphical representation, known as “feynman diagram”, of electron-electron  
 337 scattering.

338 • *Strong interaction (SI)* described by Quantum Chromodynamics (QCD). Hadrons  
 339 like proton and neutron have internal structure given that they are composed  
 340 of two or more valence quarks<sup>5</sup>. Quarks have fractional electric charge which  
 341 means that they are subject to electromagnetic interaction and in the case of the  
 342 proton they should break apart due to electrostatic repulsion; however, quarks  
 343 are held together inside the hadrons against their electrostatic repulsion by the  
 344 “Strong Force” through the exchange of “gluons.” The analog to the electric  
 345 charge is the “color charge”. Electrons and photons are elementary particles  
 346 as quarks but they don’t carry color charge, therefore they are not subject to  
 347 SI. The feynman diagram for gluon exchange between quarks is shown in figure  
 348 2.4b).

349 • *Weak interaction (WI)* described by the Weak theory (WT), is responsible for  
 350 instance for the radioactive decay in atoms and proton-proton (pp) fusion within  
 351 the sun. Quarks and leptons are the particles affected by the weak interaction

---

<sup>5</sup> particles made of four and five quarks are exotic states not so common

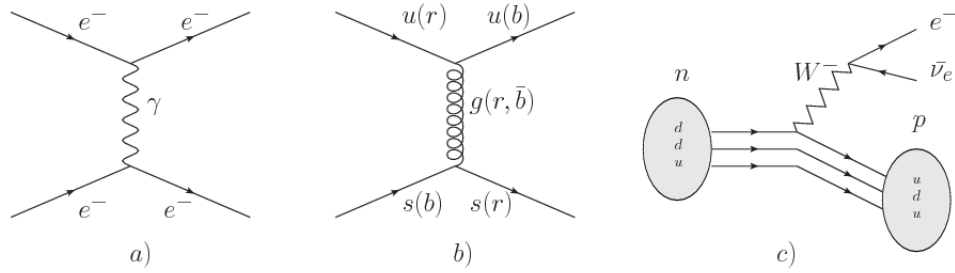


**Figure 2.4:** Feynman diagrams representing the interactions in SM; a) EI:  $e$ - $e$  scattering; b) SI: gluon exchange between quarks ; c) WI:  $\beta$ -decay

and posses a property called “flavor charge” which can be changed by emitting or absorbing one weak force mediator; they comes in six flavors each (see 2.2.1). There are three mediators of the “Weak force” known as “Z” boson in the case of electrically neutral changes and “ $W^\pm$ ” bosons in the case of electrically charged changes. The “weak isospin” is the WI analog to electric charge in EI and color charge in SI and define how quarks and leptons are affected by the weak force. Figure 2.4c) shows the feynman diagram of  $\beta$ -decay where a newtron ( $n$ ) is transformed in a proton ( $p$ ) by emmiting a  $W^-$  particle. Since this thesis is in the frame of the electroweak interaction, a more detailed description of it will be given in section 2.3

- *Gravitational interaction (GI)* described by General Theory of Relativity (GR). It is responsible for the structure of galaxies and black holes as well as the expansion of the universe. As a classical theory, in the sense that it can be formulated without even appeal to the concept of quantization, it implies that the spacetime is a continuum and predictions can be made without limitation to the precision of the measurement tools which represent a direct contradiction of the quantum mechanics principles. Gravity is deterministic while quantum mechanics is probabilistic; despite that, efforts to develop a quantum theory of

370 gravity have predicted the “graviton” as mediator of the Gravitational force<sup>6</sup>.

Interaction	Acts on	Relative strength	Range (m)	Mediators
Electromagnetic (QED)	Electrically charged particles	$10^{-2}$	Infinite	Photon
Strong (QCD)	Quarks and gluons	1	$10^{-15}$	Gluon
Weak (WI)	Leptons and quarks	$10^{-6}$	$10^{-18}$	$W^\pm, Z$
Gravitational (GI)	Massive particles	$10^{-39}$	Infinite	Graviton

**Table 2.5:** Fundamental interactions features [30].

371

372 Table 2.5 summarizes the main features of the fundamental interactions. The relative  
 373 strength of the fundamental forces reveals the meaning of strong and weak; in a  
 374 context where the relative strength of the SI is 1, the EI is about hundred times  
 375 weaker and WI is about million times weaker than the SI. A good description on  
 376 how the relative strength and range of the fundamental interactions are calculated  
 377 can be found in references [30, 31]. In the everyday life, only EI and GI are explicitly  
 378 experienced due to the range of these interactions; i.e., at the human scale distances  
 379 only EI and GI have appreciable effects, in contrast to SI which at distances greater  
 380 than  $10^{-15}$ m become negligible.

381 QED was built successfully on the basis of the classical electrodynamics theory   
 382 Maxwell and Lorentz (CED), following theoretical and experimental requirements  
 383 imposed by

- 384     • lorentz invariance: independence on the reference frame.  
 385     • locality: interacting fields are evaluated at the same space-time point to avoid  
 386       action at a distance.

---

<sup>6</sup> Actually a wide variety of theories have been developed in an attempt to describe gravity; some famous examples are string theory and supergravity.

- 387     • renormalizability: physical predictions are finite and well defined
- 388     • particle spectrum, symmetries and conservation laws already known must emerge
- 389       from the theory.
- 390     • gauge invariance.
- 391     The gauge invariance requirement reflects the fact that the fundamental fields cannot
- 392     be directly measured but associated fields which are the observables. Electric (“**E**”)
- 393     and magnetic (“**B**”) fields in CED are associated with the electric scalar potential
- 394     “V” and the vector potential “**A**”. In particular, **E** can be obtained by measuring
- 395     the change in the space of the scalar potential ( $\Delta V$ ); however, two scalar potentials
- 396     differing by a constant “f” correspond to the same electric field. The same happens
- 397     in the case of the vector potential “**A**”; thus, different configurations of the associated
- 398     fields result in the same set of values of the observables. The freedom in choosing
- 399     one particular configuration is known as “gauge freedom”; the transformation law
- 400     connecting two configurations is known as “gauge transformation” and the fact that
- 401     the observables are not affected by a gauge transformation is called “gauge invariance”.
- 402     When the gauge transformation:

$$\begin{aligned} \mathbf{A} &\rightarrow \mathbf{A} - \nabla f \\ V &\rightarrow V - \frac{\partial f}{\partial t} \end{aligned} \tag{2.5}$$

403     is applied to Maxwell equations, they are still satisfied and the fields remain invariant.

404     Thus, the classical electrodynamics theory is invariant under gauge transformations

405     and is called a “gauge theory”. The set of all gauge transformations form the “sym-

406     metry group” of the theory, which according to the group theory, has a set of “group

407 generators". The number of group generators determine the number of "gauge fields"  
 408 of the theory.

409 As mentioned in the first lines of section 2.2, QED has one symmetry group ( $U(1)$ )  
 410 with one group generator (the  $Q$  operator) and one gauge field (the electromagnetic  
 411 field  $A^\mu$ ). In CED there is not a clear definition, beyond the historical convention, of  
 412 which fields are the fundamental and which are the associated, but in QED it is clear  
 413 that the fundamental field is  $A^\mu$ . When a gauge theory is quantized, the gauge field  
 414 is quantized and its quanta is called "gauge boson". The word boson characterizes  
 415 particles with integer spin which obey Bose-Einstein statistics.

416 As will be detailed in section 2.3, interactions between particles in a system can be  
 417 obtained by considering first the Lagrangian density of free particles in the system,  
 418 which of course is incomplete because the interaction terms have been left out, and  
 419 demanding global phase transformation invariance. Global phase transformation in-  
 420 variance means that a gauge transformation is performed identically to every point in  
 421 the space<sup>7</sup> and the Lagrangian remains invariant. Then, the global transformation is  
 422 promoted to a local phase transformation (this time the gauge transformation depends  
 423 on the position in space) and again invariance is required. Due to the space depen-  
 424 dence of the local transformation, the Lagrangian density is not invariant anymore.

425 In order to restate the gauge invariance, the gauge covariant derivative is introduced  
 426 in the Lagrangian and with it the gauge field responsible for the interaction between  
 427 particles in the system. The new Lagrangian density is gauge invariant, includes the  
 428 interaction terms needed to account for the interactions and provide a way to explain  
 429 the interaction between particles through the exchange of the gauge boson.

430 This recipe was used to build QED and the theories that aim to explain the funda-  
 431 mental interactions.

---

<sup>7</sup> Here space corresponds to the 4-dimensional space i.e. space-time.

### 432 2.2.3 Gauge Bosons

433 The importance of the gauge bosons comes from the fact that they are the force  
 434 mediators or force carriers. The features of the gauge bosons reflect the features of  
 435 the fields they represent; these features are extracted from the Lagrangian density used  
 436 to describe the interactions. In section 2.3, it will be shown how the gauge bosons  
 437 of the EI and WI emerge from the electroweak Lagrangian. The SI gauge bosons  
 438 features are also extracted from the SI Lagrangian but it is not detailed in this  
 439 document. However, the main features of the SM gauge bosons will be briefly presented  
 440 and summarized in table 2.6.

441 • **Photon.** EI occurs when the photon couples to (is exchanged between) particles  
 442 carrying electric charge; however, the photon itself does not carry electric charge,  
 443 therefore, there is no coupling between photons. Given that the photon is  
 444 massless the EI is of infinite range i.e. electrically charged particles interact  
 445 even if they are located far away one from each other; this also means that  
 446 photons always move with the speed of light.

447 • **Gluon.** SI is mediated by gluons, which are like photons are massless. They  
 448 carry one unit of color charge and one unit of anticolor charge which means that  
 449 gluons couple to other gluons. As a result, the range of the SI is not infinite  
 450 but very short due to the attraction between gluons, giving rise to the “color  
 451 confinement” which explains why color charged particles cannot be isolated but  
 452 live within composite particles, like quarks inside protons.

453 • **W, Z.** The EWI mediators,  $W^\pm$  and Z, are massive which explains short-  
 454 range. Given that the WI is the only interaction that can change the flavor  
 455 of the interacting particles, the W boson is responsible for the nuclear

456 transmutation where a neutron is converted in a proton or vice versa with the  
 457 involvement of an electron and a neutrino. The Z boson is the responsible of the  
 458 neutral weak processes like neutrino elastic scattering where no electric charge  
 459 but momentum transference is involved. WI gauge bosons carry isospin charge  
 460 which makes possible the interaction between them.

Interaction	Mediator	Electric charge (e)	Color charge	Weak Isospin	mass ( $\text{GeV}/c^2$ )
Electromagnetic	Photon ( $\gamma$ )	0	No	0	0
Strong	Gluon (g)	0	Yes -octet	No	0
Weak	$W^\pm$	$\pm 1$	No	$\pm 1$	$80.385 \pm 0.015$
	Z	0	No	0	$91.188 \pm 0.002$

**Table 2.6:** SM gauge bosons main features [21].

461

## 462 2.3 Electroweak unification and the Higgs 463 mechanism

464 I physicist dreams of building a theory that contains all the interactions in one single  
 465 interaction, i.e. showing that at some scale in energy all the four fundamental in-  
 466 teractions are unified and only one interaction emerges in a “Theory of everything”.  
 467 The first sign of the feasibility of such unification comes from success in the con-  
 468 struction of the CED. Einstein spent years trying to reach that dream, which by  
 469 1920 only involved electromagnetism and gravity, with no success; however, a new  
 470 partial unification was achieved in the 1960’s, when S.Glashow [14], A.Salam [15] and  
 471 S.Weinberg [16] independently proposed that electromagnetic and weak interactions  
 472 are two manifestations of a more general interaction called “electroweak interaction.”  
 473 QCD and EW were developed in parallel and following the useful prescription pro-  
 474 vided by QED and the gauge invariance principles.

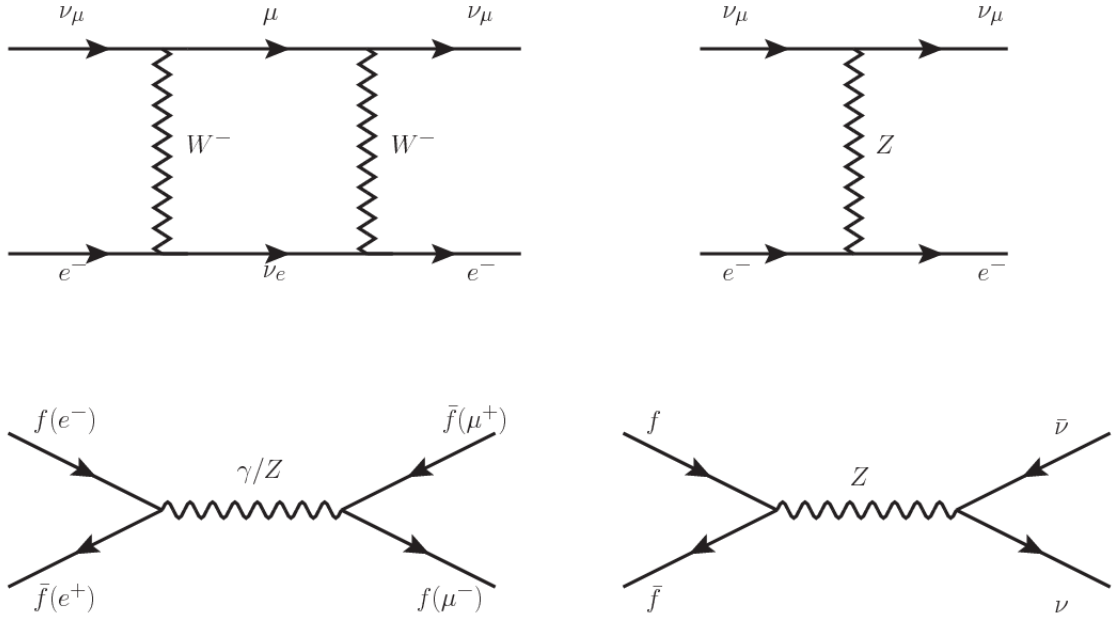


**Figure 2.5:** Top:  $\nu_\mu - e^-$  scattering going through charged currents (left) and neutral currents (right). Bottom: neutral current processes for charged fermions (left) and involving neutrinos (right). While neutral current processes involving only charged fermions can proceed through EI or WI, those involving neutrinos can only proceed via WI.

475 The theory of weak interactions was capable of explaining the  $\beta$ -decay and in general  
 476 the processes mediated by  $W^\pm$  bosons. However, there were some processes like the  
 477 “ $\nu_\mu - e$  scattering” which would require the exchange of two W bosons (see figure 2.5  
 478 top diagrams) giving rise to divergent loop integrals and then non finite predictions.  
 479 By including neutral currents involving fermions via the exchange of neutral bosons  
 480 Z, those divergences are compensated and the predictions become realistic.  
 481 Neutral weak interaction vertices conserve flavor in the same way as the electromag-  
 482 netic vertices do, but additionally, the Z boson can couple to neutrinos which implies  
 483 that processes involving charged fermions can proceed through EI or WI but processes  
 484 involving neutrinos can proceed only through WI.  
 485 The prescription to build a gauge theory of the WI consist of proposing a free field La-  
 486 grangian density that includes the particles involved; next, by requesting invariance

under global phase transformations first and generalizing to local phase transformations invariance later, the conserved currents are identified and interactions are generated by introducing gauge fields. Given that the goal is to include the EI and WI in a single theory, the group symmetry considered should be a combination of  $SU(2)_L$  and  $U(1)_{em}$ , however the latter cannot be used directly because the EI treat left and right-handed particles indistinctly in contrast to the former. Fortunately, the weak hypercharge, which is a combination of the weak isospin and the electric charge (eqn 2.3) is suitable to be used since it is conserved by the EI and WI. Thus, the symmetry group to be considered is

$$G \equiv SU(2)_L \otimes U(1)_Y \quad (2.6)$$

The following treatment applies to any of the fermion generations  for simplicity the first generation of leptons will be considered [2, 3, 32, 33]. Also, the unified weak and electromagnetic interaction will be referred as “Electroweak Interaction (EWI).”

 Given the first generation of leptons

$$\psi_1 = \begin{pmatrix} \nu_e \\ e^- \end{pmatrix}_L, \quad \psi_2 = \nu_{eR}, \quad \psi_3 = e_R^- \quad (2.7)$$

the charged fermionic currents are given by

$$J_\mu \equiv J_\mu^+ = \bar{\nu}_{eL} \gamma_\mu e_L, \quad J_\mu^\dagger \equiv J_\mu^- = \bar{e}_L \gamma_\mu \nu_{eL} \quad (2.8)$$

and the free Lagrangian is given by

$$\mathcal{L}_0 = \sum_{j=1}^3 i\bar{\psi}_j(x) \gamma^\mu \partial_\mu \psi_j(x). \quad (2.9)$$

Mass terms are included directly in the QED and QCD free Lagrangians since they

503 preserve the invariance under the symmetry transformations involved which treat  
 504 left-handed and right-handed similarly, however mass terms of the form

$$m_W^2 W_\mu^\dagger(x) W^\mu(x) + \frac{1}{2} m_Z^2 Z_\mu(x) Z^\mu(x) - m_e \bar{\psi}_e(x) \psi_e(x) \quad (2.10)$$

505 which represent the mass of  $W^\pm$ , Z and electrons, are not invariant under G trans-  
 506 formations, therefore the gauge fields described by the EWI are in principle massless.  
 507 Experiments have shown that the gauge fields are not massless; however, they have to  
 508 acquire mass through a mechanism compatible with the gauge invariance; that mech-  
 509 anism is known as the “Higgs mechanism” and will be considered later in this section.  
 510 The global transformations in the combined symme group G can be written as

$$\begin{aligned} \psi_1(x) &\xrightarrow{G} \psi'_1(x) \equiv U_Y U_L \psi_1(x), \\ \psi_2(x) &\xrightarrow{G} \psi'_2(x) \equiv U_Y \psi_2(x), \\ \psi_3(x) &\xrightarrow{G} \psi'_3(x) \equiv U_Y \psi_3(x) \end{aligned} \quad (2.11)$$

511 where  $U_L$  represent the  $SU(2)_L$  transformation acting on  weak isospin doublet  
 512 only and  $U_Y$  represent the  $U(1)_Y$  transformation acting on all the weak isospin mul-  
 513 tiplets. Explicitly

$$U_L \equiv \exp\left(i \frac{\sigma_i}{2} \alpha^i\right), \quad U_Y \equiv \exp(i y_i \beta) \quad (i = 1, 2, 3) \quad (2.12)$$

514 with  $\sigma_i$  the Pauli matrices and  $y_i$  the weak hypercharges. In order to promote the  
 515 transformations from global to local keeping the invariance, it is required that  $\alpha^i =$   
 516  $\alpha^i(x)$  and  $\beta = \beta(x)$  and the replace of the ordinary derivatives by the covariant  
 517 derivatives

$$\begin{aligned}
D_\mu \psi_1(x) &\equiv \left[ \partial_\mu + ig\sigma_i W_\mu^i(x)/2 + ig'y_1 B_\mu(x) \right] \psi_1(x) \\
D_\mu \psi_2(x) &\equiv \left[ \partial_\mu + ig'y_2 B_\mu(x) \right] \psi_2(x) \\
D_\mu \psi_3(x) &\equiv \left[ \partial_\mu + ig'y_3 B_\mu(x) \right] \psi_3(x)
\end{aligned} \tag{2.13}$$

518 introducing four gauge fields,  $W_\mu^i(x)$  and  $B_\mu(x)$ , in the process. The covariant deriva-  
519 tives (eqn 2.13) are required to transform in the same way as fermion fields  $\psi_i(x)$   
520 themselves, therefore, the gauge fields transform as:

$$\begin{aligned}
B_\mu(x) &\xrightarrow{G} B'_\mu(x) \equiv B_\mu(x) - \frac{1}{g'} \partial_\mu \beta(x) \\
W_\mu^i(x) &\xrightarrow{G} W_\mu^{i'}(x) \equiv W_\mu^i(x) - \frac{i}{g} \partial_\mu \alpha_i(x) - \varepsilon_{ijk} \alpha_i(x) W_\mu^j(x).
\end{aligned} \tag{2.14}$$

521 The G invariant version of the Lagrangian density 2.9 can be written as

$$\mathcal{L}_0 = \sum_{j=1}^3 i\bar{\psi}_j(x) \gamma^\mu D_\mu \psi_j(x) \tag{2.15}$$

522 where free massless fermion and gauge fields and fermion-gauge boson interactions  
523 are included. The EWI Lagrangian density must additionally include kinetic terms  
524 for the gauge fields ( $\mathcal{L}_G$ ) which are built from the field strengths, according to 

$$B_{\mu\nu}(x) \equiv \partial_\mu B_\nu - \partial_\nu B_\mu \tag{2.16}$$

$$W_{\mu\nu}^i(x) \equiv \partial_\mu W_\nu^i(x) - \partial_\nu W_\mu^i(x) - g\varepsilon^{ijk} W_\mu^j W_\nu^k \tag{2.17}$$

525 the last term in eqn. 2.17 is added in order to hold the gauge invariance; therefore,

$$\mathcal{L}_G = -\frac{1}{4}B_{\mu\nu}(x)B^{\mu\nu}(x) - \frac{1}{4}W_{\mu\nu}^i(x)W_i^{\mu\nu}(x) \quad (2.18)$$

526 which contains not only the free gauge fields contribution  but also the gauge fields  
 527 self-interactions and interactions among them.

528 The three weak isospin conserved currents resulting from the  $SU(2)_L$  symmetry are  
 529 given by

$$J_\mu^i(x) = \frac{1}{2}\bar{\psi}_1(x)\gamma_\mu\sigma^i\psi_1(x) \quad (2.19)$$

530 while the weak hypercharge conserved current resulting from the  $U(1)_Y$  symmetry is  
 531 given by

$$J_\mu^Y = \sum_{j=1}^3 \bar{\psi}_j(x)\gamma_\mu y_j \psi_j(x) \quad (2.20)$$

532 In order to evaluate the electroweak interactions modeled by an  triplet fields  $W_\mu^i$   
 533 which couples to isospin currents  $J_\mu^i$  with strength  $g$  and additionally the singlet  
 534 field  $B_\mu$  which couples to the weak hypercharge current  $J_\mu^Y$  with strength  $g'/2$ ,   
 535 interaction Lagrangian density to be considered is

$$\mathcal{L}_I = -g J^{i\mu}(x) W_\mu^i(x) - \frac{g'}{2} J^Y{}^\mu(x) B_\mu(x) \quad (2.21)$$

536 Note that the weak isospin currents are not the same as the charged fermionic currents  
 537 that were used to describe the WI (eqn 2.8), since the weak isospin eigenstates are  
 538 not the same as the mass eigenstates, but they are closely related

$$J_\mu = \frac{1}{2}(J_\mu^1 + iJ_\mu^2), \quad J_\mu^\dagger = \frac{1}{2}(J_\mu^1 - iJ_\mu^2). \quad (2.22)$$

539 The same happens with the gauge fields  $W_\mu^i$  which are related to the mass eigenstates  
 540  $W^\pm$  by

$$W_\mu^+ = \frac{1}{\sqrt{2}}(W_\mu^1 - iW_\mu^2), \quad W_\mu^- = \frac{1}{\sqrt{2}}(W_\mu^1 + iW_\mu^2). \quad (2.23)$$

541 The fact that there are three weak isospin conserved currents is an indication that in  
 542 addition to the charged fermionic current which couple charged to neutral leptons  
 543 there should be a neutral fermionic current that couples neutral fermions or electri-  
 544 cally charged fermions that have the same electric charge and thus does not imply  
 545 electric charge change. The third weak isospin current contains a term that is simi-  
 546 lar to the electromagnetic current ( $j_\mu^{em}$ ), indicating that there is a relation between  
 547 them and resembling the Gell-Mann-Nishijima formula 2.3 adapted to electroweak  
 548 interactions

$$Q = T_3 + \frac{Y_W}{2}. \quad (2.24)$$

549 Just as  $Q$  generates the  $U(1)_{em}$  symmetry, the weak hypercharge generates the  $U(1)_Y$   
 550 symmetry as said before. It is possible to write the relationship in terms of the currents  
 551 as

$$j_\mu^{em} = J_\mu^3 + \frac{1}{2}J_\mu^Y. \quad (2.25)$$

552 The neutral gauge fields  $W_\mu^3$  and  $B_\mu$  cannot be directly identified with the  $Z$  and the  
 553 photon fields since the photon interacts similarly with left and right-handed fermions;  
 554 however, they are related through a linear combination given by

$$A_\mu = B_\mu \cos \theta_W + W_\mu^3 \sin \theta_W \quad (2.26)$$

$$Z_\mu = -B_\mu \sin \theta_W + W_\mu^3 \cos \theta_W$$

555 where  $\theta_W$  is known as the “Weinberg angle.” The interaction Lagrangian is now given

556 by

$$\mathcal{L}_I = -\frac{g}{\sqrt{2}}(J^\mu W_\mu^+ + J^{\mu\dagger} W_\mu^-) - \left(g \sin \theta_W J_\mu^3 + g' \cos \theta_W \frac{J_\mu^Y}{2}\right) A^\mu - \left(g \cos \theta_W J_\mu^3 - g' \sin \theta_W \frac{J_\mu^Y}{2}\right) Z^\mu \quad (2.27)$$

557 the first term is the weak charged current interaction, while the second term is the

558 electromagnetic interaction under the condition

$$g \sin \theta_W = g' \cos \theta_W = e, \quad \frac{g'}{g} = \tan \theta_W \quad (2.28)$$

559 contained in the eqn.2.25; the third term is the neutral weak current.

560 Note that the neutral fields transformation given by the eqn. 2.26 can be written in

561 terms of the coupling constants  $g$  and  $g'$  as:

$$A_\mu = \frac{g' W_\mu^3 + g B_\mu}{\sqrt{g^2 + g'^2}}, \quad Z_\mu = \frac{g W_\mu^3 - g' B_\mu}{\sqrt{g^2 + g'^2}} \quad (2.29)$$

562 So far, the Lagrangian density describing the non-massive EWI is:

$$\mathcal{L}_{nmEWI} = \mathcal{L}_0 + \mathcal{L}_G \quad (2.30)$$

563 where fermion and gauge fields have been considered massless because their regular

564 mass terms are manifestly non invariant under G transformations; therefore, masses

565 have to be generated in a gauge invariant way. The mechanism by which this goal is

566 achieved is known as the “Higgs mechanism” and is closely connected to the concept  
 567 of “spontaneous symmetry breaking.”

### 568 2.3.1 Spontaneous symmetry breaking

569 Figure 2.6 left shows a steel nail (top) which is subject to an external force; the form  
 of the potential energy is also shown (bottom).

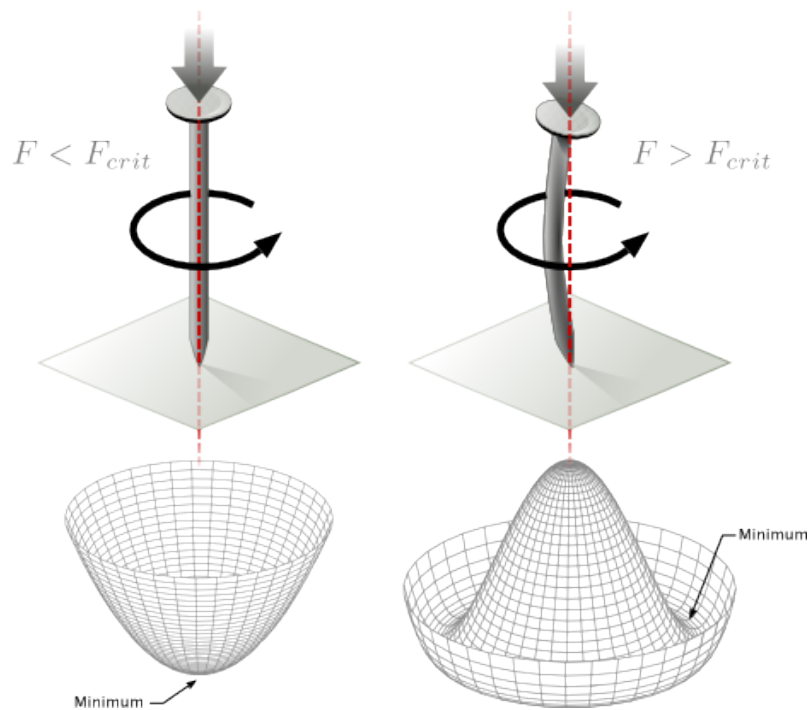


**Figure 2.6:** Spontaneous symmetry breaking mechanism. The steel nail, subject to an external force (top left), has rotational symmetry with respect to its axis. When the external force overcomes a critical value the nail buckles (top right) choosing a minimal energy state (ground state) and thus “*breaking spontaneously the rotational symmetry*”. The potential energy (bottom) changes but holds the rotational symmetry; however, an infinite number of asymmetric ground states are generated and circularly distributed in the bottom of the potential [34].

570

571 Before reaching the critical force value, the system has rotational symmetry with re-  
 572 spect to the nail axis; however, after the critical force value is reached the nail buckles  
 573 (top right). The form of the potential energy (bottom right) changes, preserving its

574 rotational symmetry although its minima  exhibit that rotational symmetry  
 575 any longer. Right before the nail buckles there is no indication of the direction the  
 576 nail will bend because any of the directions are equivalent, but once the nail bent,  
 577 choosing a direction, an arbitrary minimal energy state (ground state) is selected and  
 578 it does not share the system rotational symmetry. This mechanism for reaching an  
 579 asymmetric ground state is known as “*spontaneous symmetry breaking (SSB)*”.  
 580 The lesson from this analysis is that the way to introduce the SSB mechanism into a  
 581 system is by adding the appropriate potential to it.

582 Figure 2.7 shows a plot of the potential  $V(\phi)$  in the case of a scalar field  $\phi$

$$V(\phi) = \mu^2 \phi^\dagger \phi + \lambda (\phi^\dagger \phi)^2 \quad (2.31)$$

583 If  $\mu^2 > 0$  the potential has only one minimum at  $\phi = 0$  and describes  scalar field  
 584 with mass  $\mu$ . If  $\mu^2 < 0$  the potential has a local maximum at  $\phi = 0$  and two minima  
 585 at  $\phi = \pm\sqrt{-\mu^2/\lambda}$  which enables the SSB mechanism to work.

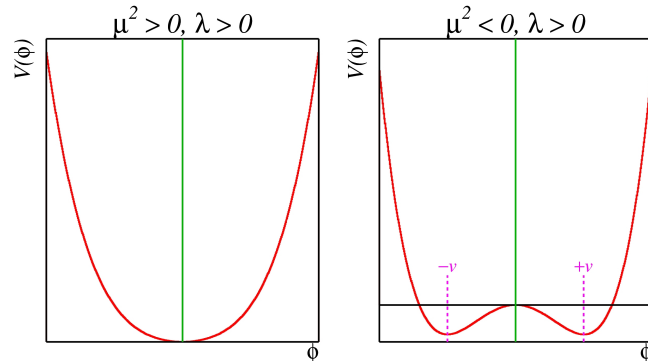


**Figure 2.7:** Shape of the potential  $V(\phi)$  for  $\lambda > 0$  and:  $\mu^2 > 0$  (left) and  $\mu^2 < 0$  (right). The case  $\mu^2 < 0$  corresponds to the potential suitable for introducing the SSB mechanism by choosing one of the two ground states which are connected via reflection symmetry. [34].

586 In the case of a complex scalar field  $\phi(x)$

$$\phi(x) = \frac{1}{\sqrt{2}}(\phi_1 + i\phi_2) \quad (2.32)$$

587 the Lagrangian (invariant under global  $U(1)$  transformations) is given by

$$\mathcal{L} = (\partial_\mu \phi)^\dagger (\partial^\mu \phi) - V(\phi), \quad V(\phi) = \mu^2 \phi^\dagger \phi + \lambda (\phi^\dagger \phi)^2 \quad (2.33)$$

588 where an appropriate potential has been added in order to introduce the SSB.

589 As seen in figure 2.8, the potential has now an infinite number of minima circularly  
 590 distributed along the  $\xi$ -direction which makes possible the occurrence of the SSB by  
 591 choosing an arbitrary ground state; for instance,  $\xi = 0$ , i.e.  $\phi_1 = v, \phi_2 = 0$

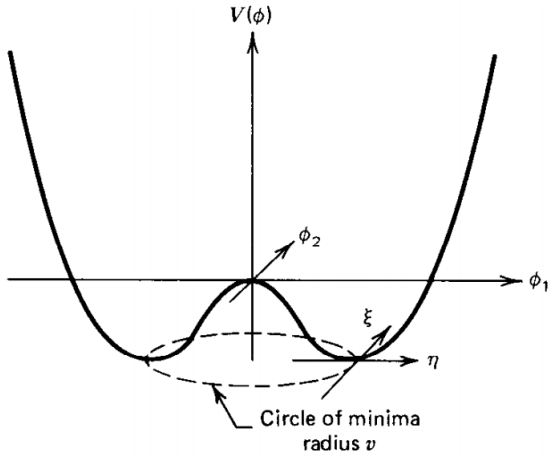


**Figure 2.8:** Potential for complex scalar field. There is a circle of minima of radius  $v$  along the  $\xi$ -direction [3].

$$\phi_0 = \frac{v}{\sqrt{2}} \exp(i\xi) \xrightarrow{\text{SSB}} \phi_0 = \frac{v}{\sqrt{2}} \quad (2.34)$$

592 As usual, excitations over the ground state are studied by making an expansion about  
 593 it; thus, the excitation can be parametrized as:

$$\phi(x) = \frac{1}{\sqrt{2}}(v + \eta(x) + i\xi(x)) \quad (2.35)$$

594 which when substituted into eqn. 2.33 produces a Lagrangian in terms of the new  
 595 fields  $\eta$  and  $\xi$

$$\mathcal{L}' = \frac{1}{2}(\partial_\mu \xi)^2 + \frac{1}{2}(\partial_\mu \eta)^2 + \mu^2 \eta^2 - V(\phi_0) - \lambda v \eta (\eta^2 + \xi^2) - \frac{\lambda}{4}(\eta^2 + \xi^2)^2 \quad (2.36)$$

596 where the last two terms represent the interactions and self-interaction between the  
 597 two fields  $\eta$  and  $\xi$ . The particular feature of the SSB mechanism is revealed when  
 598 looking to the first three terms of  $\mathcal{L}'$ . Before the SSB, only the massless  $\phi$  field is  
 599 present in the system; after the SSB there are two fields of which the  $\eta$ -field has  
 600 acquired mass  $m_\eta = \sqrt{-2\mu^2}$  while the  $\xi$ -field is still massless (see figure 2.9).

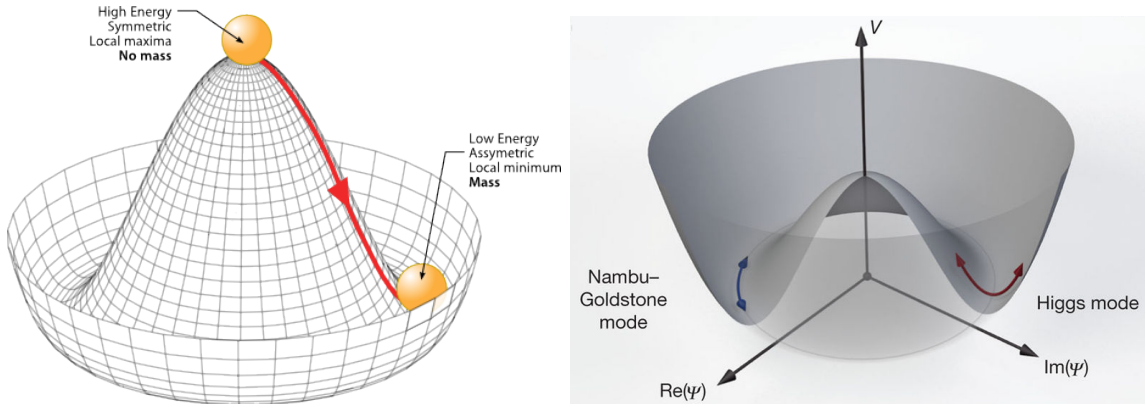


**Figure 2.9:** SSB mechanism for a complex scalar field [34, 35].

601 Thus, the SSB mechanism serves as a method to generate mass but as a side effect a  
 602 massless field is introduced in the system. This fact is known as the Goldstone theorem  
 603 and states that a massless scalar field appears in the system for each continuous  
 604 symmetry spontaneously broken. Another version of the Goldstone theorem states  
 605 that “if a Lagrangian is invariant under a continuous symmetry group  $G$ , but the  
 606 vacuum is only invariant under a subgroup  $H \subset G$ , then there must exist as many  
 607 massless spin-0 particles (Nambu-Goldstone bosons) as broken generators.” [33] The

608 Nambu-Goldstone boson can be understood considering that the potential in the  $\xi$ -  
 609 direction is flat so excitations in that direction are not energy consuming and thus  
 610 represent a massless state.

### 611 2.3.2 Higgs mechanism

612 When the SSB mechanism is introduced in the formulation of the EWI in an attempt  
 613 to generate the mass of the so far massless gauge bosons and fermions, an interesting  
 614 effect is revealed. In order to keep the G symmetry group invariance and generate  
 615 the mass of the EW gauge bosons G invariant Lagrangian density ( $\mathcal{L}_S$ ) has to be  
 616 added to the non massive EWI Lagrangian (eqn. 2.30)

$$\mathcal{L}_S = (D_\mu \phi)^\dagger (D^\mu \phi) - \mu^2 \phi^\dagger \phi - \lambda (\phi^\dagger \phi)^2, \quad \lambda > 0, \mu^2 < 0 \quad (2.37)$$

$$D_\mu \phi = \left( i\partial_\mu - g \frac{\sigma_i}{2} W_\mu^i - g' \frac{Y}{2} B_\mu \right) \phi \quad (2.38)$$

617  $\phi$  has to be an isospin doublet of complex scalar fields so it preserves the G invariance;  
 618 thus  $\phi$  can be defined as:

$$\phi = \begin{pmatrix} \phi^+ \\ \phi^0 \end{pmatrix} \equiv \frac{1}{\sqrt{2}} \begin{pmatrix} \phi_1 + i\phi_2 \\ \phi_3 + i\phi_4 \end{pmatrix}. \quad (2.39)$$

619 The minima of the potential are defined by

$$\phi^\dagger \phi = \frac{1}{2} (\phi_1^2 + \phi_2^2 + \phi_3^2 + \phi_4^2) = -\frac{\mu^2}{2\lambda}. \quad (2.40)$$

620 The choice of the ground state is critical. By choosing a ground state, invariant under  
 621  $U(1)_{em}$  gauge symmetry, the photon will remain massless and the  $W^\pm$  and  $Z$  bosons  
 622 masses will be generated which is exactly what is needed. In that sense, the best

623 choice corresponds to a weak isospin doublet with  $T_3 = -1/2$ ,  $Y_W = 1$  and  $Q = 0$   
 624 which defines a ground state with  $\phi_1 = \phi_2 = \phi_4$  and  $\phi_3 = v$ :

$$\phi_0 \equiv \frac{1}{\sqrt{2}} \begin{pmatrix} 0 \\ v \end{pmatrix}, \quad v^2 \equiv -\frac{\mu^2}{\lambda}. \quad (2.41)$$

625 where the vacuum expectation value  $v$  is fixed by the Fermi coupling  $G_F$  according  
 626 to  $v = (\sqrt{2}G_F)^{1/2} \approx 246$  GeV.

627 The G symmetry has been broken and three Nambu-Goldstone bosons will appear.  
 628 The next step is to expand  $\phi$  about the chosen ground state as:

$$\phi(x) = \frac{1}{\sqrt{2}} \exp\left(\frac{i}{v} \sigma_i \theta^i(x)\right) \begin{pmatrix} 0 \\ v + H(x) \end{pmatrix} \approx \frac{1}{\sqrt{2}} \begin{pmatrix} \theta_1(x) + i\theta_2(x) \\ v + H(x) - i\theta_3(x) \end{pmatrix} \quad (2.42)$$

629 to describe fluctuations from the ground state  $\phi_0$ . The fields  $\theta_i(x)$  represent the  
 630 Nambu-Goldstone bosons while  $H(x)$  is known as “higgs field.” The fundamental  
 631 feature of the parametrization used is that the dependence on the  $\theta_i(x)$  fields is  
 632 factored out in a global phase that can be eliminated by taking the physical “unitary  
 633 gauge”  $\theta_i(x) = 0$ . Therefore the expansion about the ground state is given by:

$$\phi(x) \frac{1}{\sqrt{2}} \begin{pmatrix} 0 \\ v + H(x) \end{pmatrix} \quad (2.43)$$

634 which when substituted into  $\mathcal{L}_S$  (eqn. 2.37) results in a Lagrangian containing the now  
 635 massive three gauge bosons  $W^\pm, Z$ , one massless gauge boson (photon) and the new  
 636 Higgs field ( $H$ ). The three degrees of freedom corresponding to the Nambu-Goldstone  
 637 bosons are now integrated into the massive gauge bosons as their longitudinal polar-  
 638 izations which were not available when they were massless particles. The effect by  
 639 which vector boson fields acquire mass after an spontaneous symmetry breaking but  
 640 without an explicit gauge invariance breaking is known as the “*Higgs mechanism*.”

641 The mechanism was proposed by three independent groups: F.Englert and R.Brout  
 642 in August 1964 [36]; P.Higgs in October 1964 [37]; and G.Guralnik, C.Hagen and  
 643 T.Kibble in November 1964 [38]; however, its importance was not realized until  
 644 S.Glashow [14], A.Salam [15] and S.Weinberg [16]  independently proposed that elec-  
 645 tromagnetic and weak interactions are two manifestations of a more general interac-  
 646 tion called “electroweak interaction” in 1967.

### 647 2.3.3 Masses of the gauge bosons

648 The mass of the gauge bosons is extracted by evaluating the kinetic part of Lagrangian  
 649  $\mathcal{L}_S$  in the ground state (known also as the vacuum expectation value) 

$$\left| \left( \partial_\mu - ig \frac{\sigma_i}{2} W_\mu^i - i \frac{g'}{2} B_\mu \right) \phi_0 \right|^2 = \left( \frac{1}{2} v g \right)^2 W_\mu^+ W^{-\mu} + \frac{1}{8} v^2 (W_\mu^3, B_\mu) \begin{pmatrix} g^2 & -gg' \\ -gg' & g'^2 \end{pmatrix} \begin{pmatrix} W^{3\mu} \\ B^\mu \end{pmatrix} \quad (2.44)$$

650 comparing with the typical mass term for a charged boson  $M_W^2 W^+ W^-$

$$M_W = \frac{1}{2} v g. \quad (2.45)$$

The second term in the right side of the eqn.2.44 comprises the masses of the neutral bosons, but it needs to be written in terms of the gauge fields  $Z_\mu$  and  $A_\mu$  in order to be compared to the typical mass terms for neutral bosons, therefore using eqn. 2.29

$$\begin{aligned} \frac{1}{8} v^2 [g^2 (W_\mu^3)^2 - 2gg' W_\mu^3 B^\mu + g'^2 B_\mu^2] &= \frac{1}{8} v^2 [g W_\mu^3 - g' B_\mu]^2 + 0[g' W_\mu^3 + g B_\mu]^2 \quad (2.46) \\ &= \frac{1}{8} v^2 [\sqrt{g^2 + g'^2} Z_\mu]^2 + 0[\sqrt{g^2 + g'^2} A_\mu]^2 \end{aligned}$$

651 and then

$$M_Z = \frac{1}{2}v\sqrt{g^2 + g'^2}, \quad M_A = 0 \quad (2.47)$$

### 652 2.3.4 Masses of the fermions

653 The lepton mass terms can be generated by introducing a gauge invariant Lagrangian  
 654 term describing the Yukawa coupling between the lepton field and the Higgs field 

$$\mathcal{L}_{Yl} = -G_l \left[ (\bar{\nu}_l, \bar{l})_L \begin{pmatrix} \phi^+ \\ \phi^0 \end{pmatrix} l_R + \bar{l}_R (\phi^-, \bar{\phi}^0) \begin{pmatrix} \nu_l \\ l \end{pmatrix} \right], \quad l = e, \mu, \tau. \quad (2.48)$$

655 After the SSB and replacing the usual field expansion about the ground state (eqn.2.41)  
 656 into  $\mathcal{L}_{Yl}$ , the mass term arises

$$\mathcal{L}_{Yl} = -m_l(\bar{l}_L l_R + \bar{l}_R l_L) - \frac{m_l}{v}(\bar{l}_L l_R + \bar{l}_R l_L)H = -m_l \bar{l}l \left(1 + \frac{H}{v}\right) \quad (2.49)$$

657 where the additional term represents the lepton-Higgs interaction. The quark masses  
 $m_l = \frac{G_l}{\sqrt{2}}v$  (2.50)

658 where the additional term represents the lepton-Higgs interaction. The quark masses  
 659 are generated in a similar way as lepton masses but for the upper member of the  
 660 quark doublet a different Higgs doublet is needed:

$$\phi_c = -i\sigma_2\phi^* = \begin{pmatrix} -\bar{\phi}^0 \\ \phi^- \end{pmatrix}. \quad (2.51)$$

661 Additionally, given that the quark isospin doublets are not constructed in terms of  
 662 the mass eigenstates but in terms of the flavor eigenstates  shown in table 2.4, the  
 663 coupling parameters will be related to the CKM matrix elements; thus the quark  
 664 Lagrangian is given by:

$$\mathcal{L}_{Yq} = -G_d^{i,j}(\bar{u}_i, \bar{d}'_i)_L \begin{pmatrix} \phi^+ \\ \phi^0 \end{pmatrix} d_{jR} - G_u^{i,j}(\bar{u}_i, \bar{d}'_i)_L \begin{pmatrix} -\bar{\phi}^0 \\ \phi^- \end{pmatrix} u_{jR} + h.c. \quad (2.52)$$

with  $i,j=1,2,3$ . After SSB and expansion about the ground state, the diagonal form of  $\mathcal{L}_{Yq}$  is:

$$\mathcal{L}_{Yq} = -m_d^i \bar{d}_i d_i \left(1 + \frac{H}{v}\right) - m_u^i \bar{u}_i u_i \left(1 + \frac{H}{v}\right) \quad (2.53)$$

Fermion masses depend on arbitrary couplings  $G_l$  and  $G_{u,d}$  and are not predicted by the theory.

### 2.3.5 The Higgs field

After the characterization of the fermions and gauge bosons as well as their interactions, it is necessary to characterize the Higgs field itself. The Lagrangian  $\mathcal{L}_S$  in eq. 37 written in terms of the gauge bosons is given by

$$\mathcal{L}_S = \frac{1}{4} \lambda v^4 + \mathcal{L}_H + \mathcal{L}_{HV} \quad (2.54)$$

$$\mathcal{L}_H = \frac{1}{2} \partial_\mu H \partial^\mu H - \frac{1}{2} m_H^2 H^2 - \frac{1}{2v} m_H^2 H^3 - \frac{1}{8v^2} m_H^2 H^4 \quad (2.55)$$

$$\mathcal{L}_{HV} = m_H^2 W_\mu^+ W^{\mu-} \left(1 + \frac{2}{v} H + \frac{2}{v^2} H^2\right) + \frac{1}{2} m_Z^2 Z_\mu Z^\mu \left(1 + \frac{2}{v} H + \frac{2}{v^2} H^2\right) \quad (2.56)$$

Property	Value
Electric charge	0
Colour charge	0
Spin	0
Weak isospin	-1/2
Weak hypercharge	1
Parity	1
Mass ( $\text{GeV}/c^2$ )	$125.09 \pm 0.21 \text{ (stat.)} \pm 0.11 \text{ (syst.)}$

**Table 2.7:** Higgs boson properties. Higgs mass is not predicted by the theory and the value here corresponds to the experimental measurement.

676 The mass of the Higgs boson is deduced as usual from the mass term in the Lagrangian  
 677 resulting in:

$$m_H = \sqrt{-2\mu^2} = \sqrt{2\lambda}v \quad (2.57)$$

678 however, it  is not predicted by the theory. The experimental efforts to find the  
 679 Higgs boson, carried out by the CMS and ATLAS experiments<sup>8</sup>, gave great results  
 680 by July of 2012 when the discovery of a new particles was announced and which  
 681 is compatible with the Higgs boson predicted by the electroweak theory [39, 40].  
 682 Although at the announcement time there were some reservations about calling the  
 683 new particle the “Higgs boson”, today this name is widely accepted. The result of  
 684 the measurement of the Higgs mass reported by both experiments [41] is in table 2.7.

### 685 2.3.6 Higgs boson production mechanisms at LHC.

686 This thesis explore the Higgs production at LHC; therefore the overview presented  
 687 here will be oriented specifically to the production mechanisms after pp collisions at  
 688 LHC.

689 The pp collision at..... to be completed...

690 . . . . .

691 As shown in eqns 2.48, 2.52 and 2.56, the strength of the Higgs-fermion interaction  
 692 is proportional to the fermion mass while the strength of the Higgs-gauge boson  
 693 interaction is proportional to the square of the gauge boson mass, which implies  
 694 that the Higgs production and decay mechanisms are dominated by couplings  $H -$   
 695  $(W, Z, t, b, \tau)$ .

696 In physics, a common approach to study complex systems  in starting with  
 697 a simpler version of them, for which a well known description is available, and add

---

<sup>8</sup> CMS stands for Compact Muon Solenoid; ATLAS stand for A Toroidal LHC Apparatus. Both are general experiments held at the Large Hadron Collider(LHC)

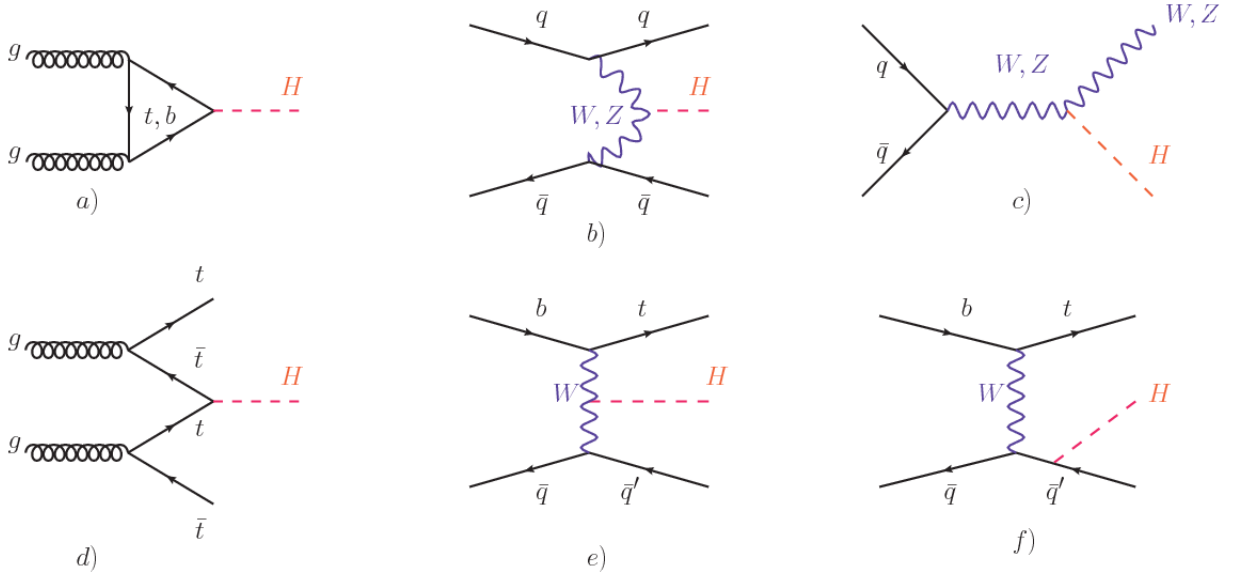


**Figure 2.10:** Main Higgs production mechanism Feynman diagrams. a) gluon-gluon fusion, b) vector boson fusion (VBF), c) Higgs-strahlung, d) Associated production with a top or bottom quark pair, e-f) associated production with a single top quark.

698 an additional “perturbation” which represent a small deviation from the known be-  
 699 havior. If the perturbation is small enough, the physical quantities associated with  
 700 the perturbed system are expressed as a series of corrections to those of the simpler  
 701 system; therefore, the more terms are considered in the series (the higher order in the  
 702 perturbation series), the more precise is the the description of the complex system.  
 703 Figure 2.10 shows the Feynman diagrams for the leading order (first order) Higgs  
 704 production processes at LHC, while the cross section for Higgs production as a func-  
 705 tion of the center of mass-energy ( $\sqrt{s}$ ) for pp collisions is showed in figure 2.11 left.  
 706 The tags NLO (next to leading order), NNLO (next to next to leading order) and  
 707 N3LO (next to next to next to leading order) make reference to the order at which  
 708 the perturbation series has been considered.  
 709 The main production mechanism is the gluon fusion ( $pp \rightarrow H$ ) given that gluons carry  
 710 the highest fraction of momentum of the protons in pp colliders. Since the Higgs boson  
 711 does not couple to gluons, the mechanism proceeds through the exchange of a virtual

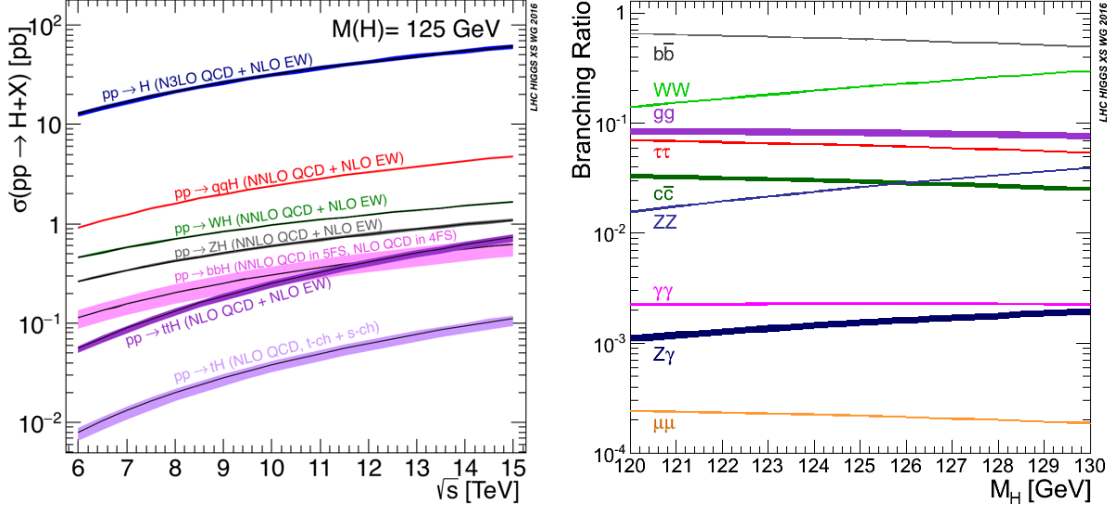


**Figure 2.11:** Higgs production cross sections (left) and decay branching ratios (right) for the main mechanisms. The VBF is indicated as  $qqH$  [42].

712 top-quark loop given that for it the coupling is the biggest. Note that in this process,  
 713 the Higgs boson is produced alone, which makes this mechanism experimentally clean  
 714 when combined with the two-photon or the four-lepton decay channels (see section  
 715 2.3.7).

716 Vector boson fusion ( $pp \rightarrow qqH$ ) has the second largest production cross section. The  
 717 scattering of two fermions is mediated by a weak gauge boson which later emits a Higgs  
 718 boson. In the final state, the two fermions tend to be located in a particular region  
 719 of the detector which is used as a signature when analyzing the datasets provided by  
 720 the experiments. More details about how to identify events of interest in an analysis  
 721 will be given in chapter 4.

722 The next production mechanism is Higgs-strahlung ( $pp \rightarrow WH, pp \rightarrow ZH$ ) where two  
 723 fermions annihilate to form a weak gauge boson. If the initial fermions have enough  
 724 energy, the emergent boson eventually will emit a Higgs boson.

725 The associated production with a top or bottom quark pair and the associated pro-  
 726 duction with a single top quark ( $pp \rightarrow bbH, pp \rightarrow t\bar{t}H, pp \rightarrow tH$ ) have a smaller cross

section than the main three mechanisms above, but they provide a good opportunity to test the Higgs-top coupling. The analysis reported in this thesis is developed using these production mechanisms. A detailed description of the  $tH$  mechanism will be given in section 2.4.

### 2.3.7 Higgs decay channels

When a particle can decay through several modes, also known as channels, the probability of decaying through a given channel is quantified by the “branching ratio” (BR) of the decay channel; thus, the BR is defined as the ratio of number of decays going through that given channel to the total number of decays. In regard to the Higgs boson decay, the BR can be predicted with accuracy once the Higgs mass is known [43, 44]. In figure 2.11 right, a plot of the BR as a function of the Higgs mass is presented. The largest BR corresponds to the  $b\bar{b}$  pair decay channel (see table 2.8).

Decay channel	Branching ratio	Rel. uncertainty
$H \rightarrow \gamma\gamma$	$2.27 \times 10^{-3}$	$+5.0\% - 4.9\%$
$H \rightarrow ZZ$	$2.62 \times 10^{-2}$	$+4.3\% - 4.1\%$
$H \rightarrow W^+W^-$	$2.14 \times 10^{-1}$	$+4.3\% - 4.2\%$
$H \rightarrow \tau^+\tau^-$	$6.27 \times 10^{-2}$	$+5.7\% - 5.7\%$
$H \rightarrow b\bar{b}$	$5.84 \times 10^{-1}$	$+3.2\% - 3.3\%$
$H \rightarrow Z\gamma$	$1.53 \times 10^{-3}$	$+9.0\% - 8.9\%$
$H \rightarrow \mu^+\mu^-$	$2.18 \times 10^{-4}$	$+6.0\% - 5.9\%$

**Table 2.8:** Branching ratios and the relative uncertainty for a SM Higgs boson with  $m_H = 125 GeV/c^2$ . [21]

740 **2.4 Associated Production of Higgs Boson and  
741 Single Top Quark.**

742 **2.5 The CP-mixing phase**

<sup>743</sup> **Chapter 3**

<sup>744</sup> **The CMS experiment at the LHC**

<sup>745</sup> Located in the Swiss-French border, the European Council for Nuclear Research  
<sup>746</sup> (CERN) is the largest scientific organization leading the particle physics research;  
<sup>747</sup> about 13000 people in a broad range of fields including users, students, scientist, en-  
<sup>748</sup> gineers among others, contribute to the data taking and analysis, with the goal of  
<sup>749</sup> unveil the secrets of the nature and reveal the fundamental structure of the universe.

<sup>750</sup> CERN is also the home of the Large Hadron Collider (LHC), the largest circular  
<sup>751</sup> particle accelerator around the world, where protons (or heavy ions) traveling close  
<sup>752</sup> to the speed of light are made to collide together. These collisions open a window to  
<sup>753</sup> investigate how particles (and their constituents if they are composite) interact with  
<sup>754</sup> each other, providing clues about the laws of the nature.

<sup>755</sup> LHC can run in three modes depending on the particles being accelerated:

- <sup>756</sup>     • Proton-Proton collisions (pp) mostly general purpose experiments.  
<sup>757</sup>     • Lead-Lead collisions (Pb-Pb) Heavy ion experiments.  
<sup>758</sup>     • Proton-Lead collisions (p-Pb).

759 There are several accelerating stages before the injection to the LHC ring. In the  
760 pp mode, after removing the electrons from Hydrogen atoms in a bottle, protons are  
761 accelerated in the LINAC2 to 50MeV and then injected into the proton synchrotron  
762 booster (BOOSTER) to reach 1.4 GeV in energy. The next boost is provided at the  
763 proton synchrotron(PS) up to 26 GeV, followed by the injection to the super proton  
764 synchrotron (SPS) where protons are accelerated to 450 GeV. Finally, protons are  
765 injected in the LHC where they are accelerated to the target energy of 6.5 TeV. In  
766 the Pb-Pb mode, the Lead ions are first accelerated in the LINAC3 and then passed as  
767 long pulses to the Low energy ion ring (LEIR) to be converted into short and dense  
768 bunches, each containing  $7 \times 10^7$  lead ions. LEIR accelerate the bunches from 4.2  
769 MeV to 72 MeV. The ions are then passed to the PS to follow the rest of acceleration  
770 process up to 2.8TeV/n en the LHC ring. Figure 3.1 show an overview of the CERN  
771 accelerating complex.

### 772 3.1 The LHC

773 The LHC is a 27 km ring composed by superconducting magnets and accelerating  
774 structures (among other components) which boost the particles traveling inside it. It  
775 is installed in the same tunnel where the large electron-positron (LEP) collider were  
776 located, taking advantage of the existing infraestructure as shown in the figure 3.2.  
777 Two particle beams travel counter-rotating in two separed beam pipes kept at ultra  
778 high vacuum. In 2008, the first set of collisions involved protons with center-of-mass  
779 energy of 7 TeV after which the energy was increased to 8 TeV in 2012 and to 13 TeV  
780 in 2015.

781 In order to keep the protons in the circular trajectory carrying that amount of  
782 energy, strong magnetic fields are needed, bringing the superconductivity into scene.

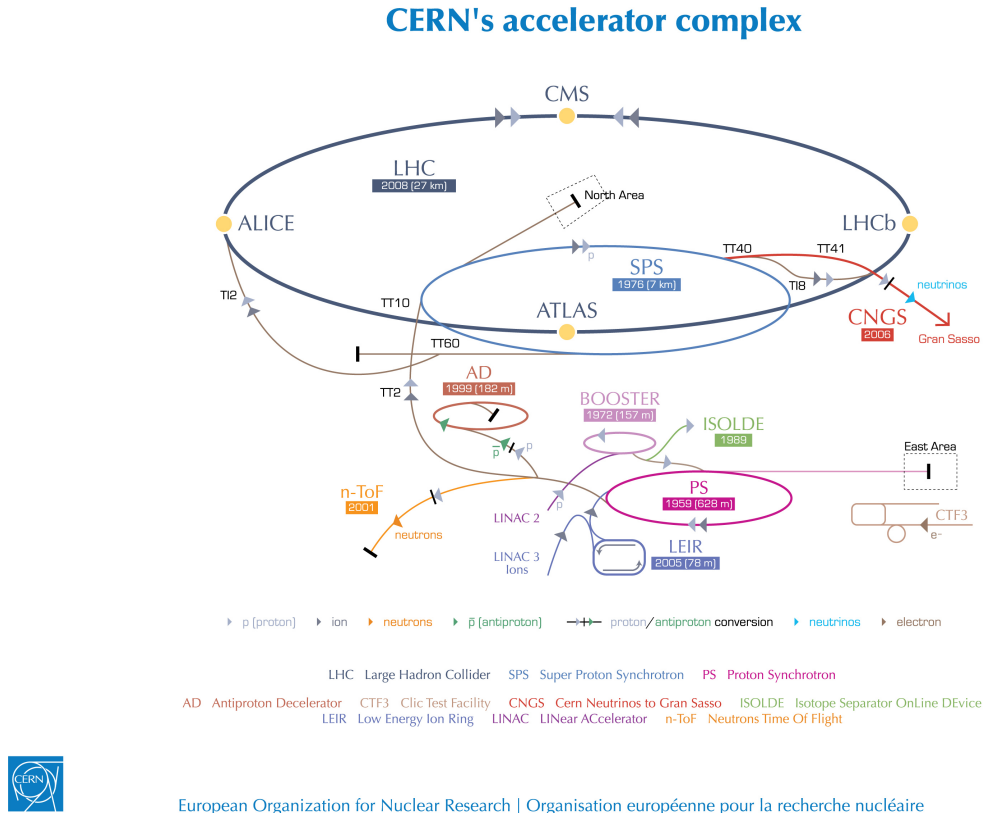
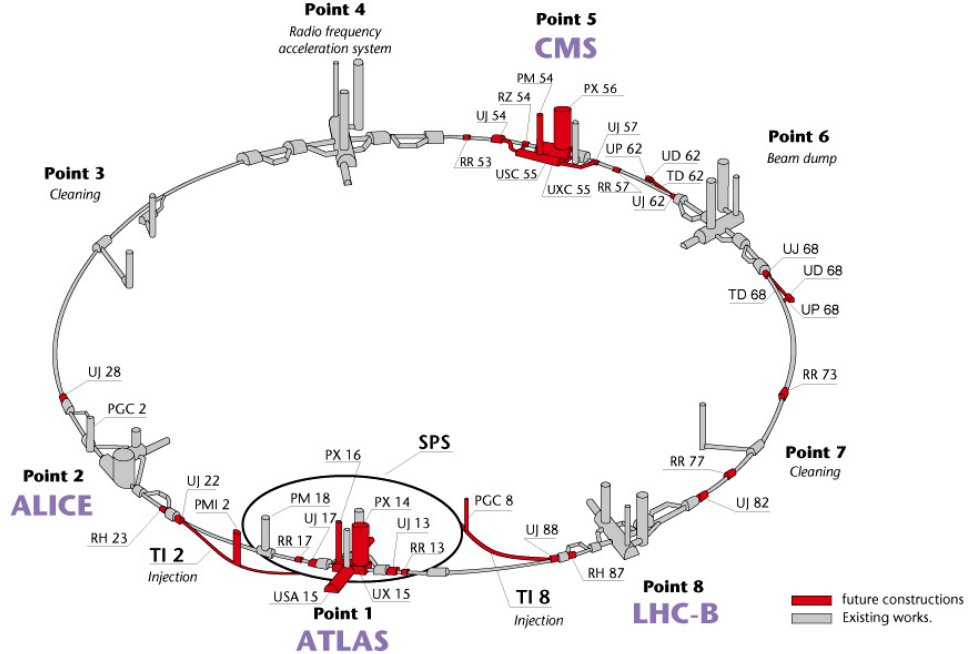


**Figure 3.1:** ref. C.Lefevre, “The CERN accelerator complex,” (2008). CERN-DI-0812015.

783 The superconducting dipole magnets used in LHC are made of a NbTi alloy, capable  
 784 to transport currents of about  $12000A$  when cooled at a temperature below  $2K$  by  
 785 using liquid helium; that current generates a magnetic fields of 8.3 T. Figure 3.3 show  
 786 the transverse view of the LHC dipole magnets. Additionally, quadrupolar magnets  
 787 are used to focus the beam and some other magnetic multipoles are used to correct  
 788 effects generated by the interaction among protons in the beam as well as interactions  
 789 within the beam pipe.

790 Regarding to the longitudinal acceleration of the protons, a system of 16 radio-  
 791 frecuency cavities (RF) (8 per beam) is used; Inside the cavities, the electromagnetic  
 792 waves become resonant transferring the maximum energy to the particle flight through  
 793 it. Cavities are cooled at 4.5 K. On LHC the RF oscillation frecuency is 400MHz and

### Layout of the LEP tunnel including future LHC infrastructures.



CERN AC \_ hf238 \_ V02/02/98

**Figure 3.2:** ref. J.-L. Caron , “Layout of the LEP tunnel including future LHC infrastructures.. L’ensemble du tunnel LEP avec les futures infrastructures LHC.”, <https://cds.cern.ch/record/841542> (Nov, 1993). AC Collection. Legacy of AC. Pictures from 1992 to 2002..

794 the protons are carefully timed so additionally to the acceleration effect the bunch  
 795 structure of the beam is preserved. The Beam is made of 2808 “bunches” which are  
 796 packages of  $1.15 \times 10^{11}$  protons ???. If LHC is at full energy, protons with the right  
 797 energy does not feel any accelerating force but those with a different energy will be  
 798 accelerated or decelerated to keep them in the bunch. The paths followed by particles  
 799 during the acceleration process are shown in figure 3.1.

800 Once the beams reach the desired energy, they are brought to cross each other  
 801 producing proton-proton collisions. The bunch crossing happens in precise places  
 802 where the LHC experiments are located. As seen in figure 3.2, it was needed to

### LHC DIPOLE : STANDARD CROSS-SECTION

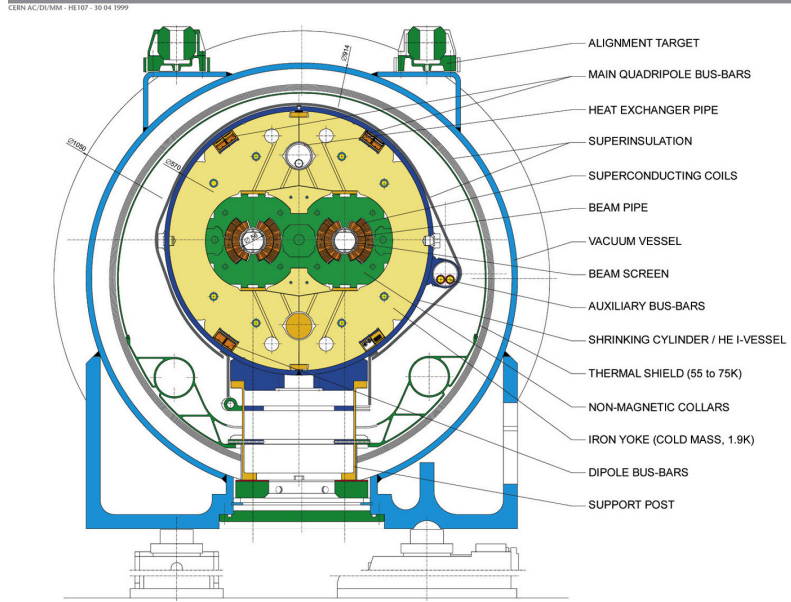


**Figure 3.3:** ref. ACTeam, “Diagram of an LHC dipole magnet. Schéma d’un aimant dipôle du LHC,” (1999). CERN-DI-9906025.

803 build the caverns for CMS and ATLAS as well as some additional facilities, but  
 804 most of the initial LEP infrastructure has been used to allocate additional collision  
 805 points. The highest luminosity is delivered at the CMS (point 5) and ATLAS (point  
 806 1) experiments, which are general purpose experiments, enabled to explore physics  
 807 in any of the collision modes. LHCb (point 8) experiment is optimized to explore  
 808 B-physics, while ALICE (point 2) is optimized for heavy ion collisions researches;  
 809 TOTEM (point 5) and LHCf (point 1) are dedicated to forward physics studies and  
 810 MoEDAL (point 8) is intended for monopoles or massive pseudo stable particles  
 811 studies.

## 812 3.2 The CMS experiment

813 The Compact Muon Solenoid (CMS) is a general purpose detector designed to conduct  
 814 research in a wide range of physics from standard model to new physics like extra

dimensions and dark matter. Located at the point 5 in the LHC layout as shown in figure 3.2, CMS is composed by several detection systems distributed in a cylindrical structure where the main feature is a solenoid magnet made of superconducting cable capable to generate a 3.8 T magnetic field. In total, CMS weight about 14000 tons in a very compact 21.6 m long and 14.6 m diameter cylinder (include a reference for CMS TDR). It was built in 15 separated sections at the ground level and lowered to the cavern individually to be assembled. Figure 3.4 show the layout of the CMS detector (CMS TDR).

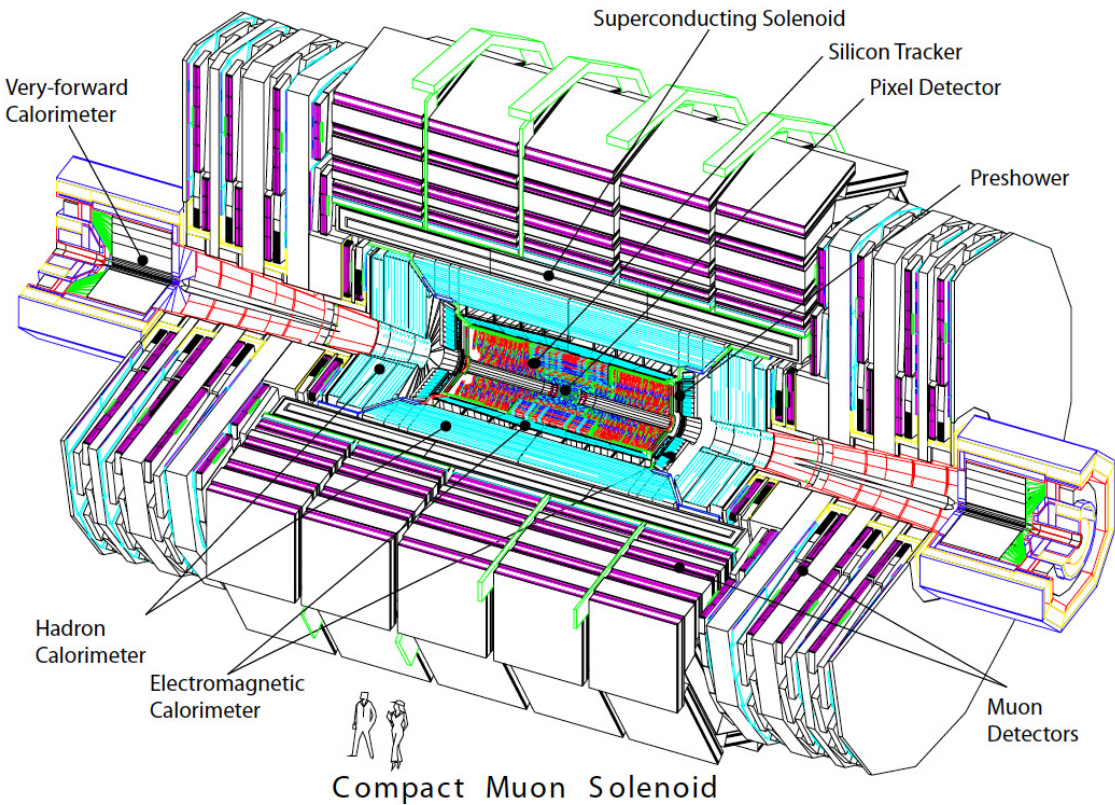


**Figure 3.4:** ref: CMS Collaboration, “Detector Drawings”, CMS-PHO-GEN-2012-002, <http://cds.cern.ch/record/1433717>, 2012.

823 **Chapter 4**

824 **Search for production of a Higgs**

825 **boson and a single top quark in**

826 **multilepton final states in pp**

827 **collisions at  $\sqrt{s} = 13$  TeV**

828 **4.1 Introduction**

829 This chapter present the search for the associated production of a Higgs boson and  
830 a single top quark events with three leptons in the final state, targeting Higgs decay  
831 modes to  $WW$ ,  $ZZ$ , and  $\tau\tau$ . The analysis uses the 13 TeV dataset produced in 2016,  
832 corresponding to an integrated luminosity of  $35.9\text{fb}^{-1}$ . It is based on and expands  
833 previous analyses at 8 TeV [45, 46] and searches for associated production of  $t\bar{t}$  and  
834 Higgs in the same channel [47], and complements searches in other decay channels  
835 targeting  $H \rightarrow b\bar{b}$  [48].

836 The production cross section of the single top plus Higgs boson ( $tHq$ ) process

837 is driven by a destructive interference of two main diagrams (see Fig. 4.1), where  
 838 the Higgs couples to either the W boson or the top quark. Any deviation from the  
 839 standard model (SM) in the Higgs coupling structure could therefore lead to a large  
 840 enhancement of the cross section, making this analysis sensitive to such deviations.  
 841 A second process, where the Higgs and top quark are accompanied by a W boson  
 842 ( $tHW$ ) has similar behavior, albeit with a weaker interference pattern.

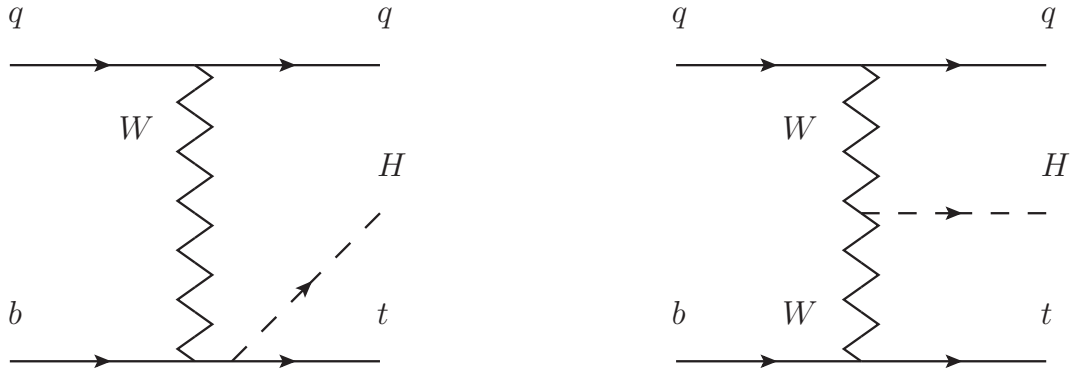


**Figure 4.1:** The two leading-order diagrams of  $tHq$  production.

843 We select events with three leptons and a  $b$  tagged jet in the final state. The  $tHq$   
 844 signal contribution is then determined in a fit of the observed data to two multivariate  
 845 classifier outputs, each trained to discriminate against one of the two dominant back-  
 846 grounds of events with non-prompt leptons from  $t\bar{t}$  and of associated production of  $t\bar{t}$   
 847 and vector bosons ( $t\bar{t}W$ ,  $t\bar{t}Z$ ). The fit result is then used to set an upper limit on the  
 848 combined  $t\bar{t}H$ ,  $tHq$  and  $tHW$  production cross section, as a function of the relative  
 849 coupling strengths of Higgs and top quark and Higgs and W boson, respectively.

## 850 4.2 Data and MC Samples

851 The data considered in this analysis were collected by the CMS experiment dur-  
 852 ing 2016 and correspond to a total integrated luminosity of  $35.9\text{fb}^{-1}$ . Only periods  
 853 when the CMS magnet was on were considered when selecting the data samples, that  
 854 corresponds to the 23 Sep 2016 (Run B to G) and PromptReco (Run H) versions  
 855 of the datasets. The MC samples used in this analysis correspond to the RunI-  
 856 ISummer16MiniAODv2 campaign produced with CMSSW 80X. The two signal sam-  
 857 ples (for  $tHq$  and  $tHW$ ) were produced with MG5\_aMC@NLO (version 5.222), in  
 858 leading-order mode, and are normalized to next-to-leading-order cross sections,  
 859 see Tab. 4.1. Each sample is generated with a set of event weights corresponding to  
 860 different values of  $\kappa_t$  and  $\kappa_V$  couplings as shown in Tab. 4.2.

### 861 4.2.1 Full 2016 dataset and MC samples

Sample	$\sigma$ [pb]	BF
/THQ_Hincl_13TeV-madgraph-pythia8_TuneCUETP8M1/	0.7927	0.324
/THW_Hincl_13TeV-madgraph-pythia8_TuneCUETP8M1/	0.1472	1.0

**Table 4.1:** Signal samples and their cross section and branching fraction used in this analysis. See Ref. [49] for more details.

862 Different MC generators were used to generate the background processes. The  
 863 dominant sources ( $t\bar{t}$ ,  $t\bar{t}W$ ,  $t\bar{t}Z$ ,  $t\bar{t}H$ ) were produced using AMC@NLO interfaced  
 864 to PYTHIA8, and are scaled to NLO cross sections. Other processes are simulated  
 865 using POWHEG interfaced to PYTHIA, or bare PYTHIA (see table 4.3 and [47]  
 866 for more details).

		$tHq$			$tHW$		
$\kappa_V$	$\kappa_t$	sum of weights	cross section [pb]	sum of weights	cross section [pb]	LHE weights	
1.0	-3.0	35.700022	2.991	11.030445	0.6409	LHEweight_wgt[446]	
1.0	-2.0	20.124298	1.706	5.967205	0.3458	LHEweight_wgt[447]	
1.0	-1.5	14.043198	1.205	4.029093	0.2353	LHEweight_wgt[448]	
1.0	-1.25	11.429338	0.9869	3.208415	0.1876	LHEweight_wgt[449]	
1.0	-1.0		0.7927		0.1472		
1.0	-0.75	7.054998	0.6212	1.863811	0.1102	LHEweight_wgt[450]	
1.0	-0.5	5.294518	0.4723	1.339886	0.07979	LHEweight_wgt[451]	
1.0	-0.25	3.818499	0.3505	0.914880	0.05518	LHEweight_wgt[452]	
1.0	0.0	2.627360	0.2482	0.588902	0.03881	LHEweight_wgt[453]	
1.0	0.25	1.719841	0.1694	0.361621	0.02226	LHEweight_wgt[454]	
1.0	0.5	1.097202	0.1133	0.233368	0.01444	LHEweight_wgt[455]	
1.0	0.75	0.759024	0.08059	0.204034	0.01222	LHEweight_wgt[456]	
1.0	1.0	0.705305	0.07096	0.273617	0.01561	LHEweight_wgt[457]	
1.0	1.25	0.936047	0.0839	0.442119	0.02481	LHEweight_wgt[458]	
1.0	1.5	1.451249	0.1199	0.709538	0.03935	LHEweight_wgt[459]	
1.0	2.0	3.335034	0.2602	1.541132	0.08605	LHEweight_wgt[460]	
1.0	3.0	10.516125	0.8210	4.391335	0.2465	LHEweight_wgt[461]	
<hr/>							
1.5	-3.0	45.281492	3.845	13.426212	0.7825	LHEweight_wgt[462]	
1.5	-2.0	27.606715	2.371	7.809713	0.4574	LHEweight_wgt[463]	
1.5	-1.5	20.476088	1.784	5.594971	0.3290	LHEweight_wgt[464]	
1.5	-1.25	17.337465	1.518	4.635978	0.2749	LHEweight_wgt[465]	
1.5	-1.0	14.483302	1.287	3.775902	0.2244	LHEweight_wgt[466]	
1.5	-0.75	11.913599	1.067	3.014744	0.1799	LHEweight_wgt[467]	
1.5	-0.5	9.628357	0.874	2.352505	0.1410	LHEweight_wgt[468]	
1.5	-0.25	7.627574	0.702	1.789184	0.1081	LHEweight_wgt[469]	
1.5	0.0	5.911882	0.5577	1.324946	0.08056	LHEweight_wgt[470]	
1.5	0.25	4.479390	0.4365	0.959295	0.05893	LHEweight_wgt[471]	
1.5	0.5	3.331988	0.3343	0.692727	0.04277	LHEweight_wgt[472]	
1.5	0.75	2.469046	0.2558	0.525078	0.03263	LHEweight_wgt[473]	
1.5	1.0	1.890565	0.2003	0.456347	0.02768	LHEweight_wgt[474]	
1.5	1.25	1.596544	0.1689	0.486534	0.02864	LHEweight_wgt[475]	
1.5	1.5	1.586983	0.1594	0.615638	0.03509	LHEweight_wgt[476]	
1.5	2.0	2.421241	0.2105	1.170602	0.06515	LHEweight_wgt[477]	
1.5	3.0	7.503280	0.5889	3.467546	0.1930	LHEweight_wgt[478]	
<hr/>							
0.5	-3.0	27.432685	2.260	8.929074	0.5136	LHEweight_wgt[479]	
0.5	-2.0	13.956013	1.160	4.419093	0.2547	LHEweight_wgt[480]	
0.5	-1.5	8.924438	0.7478	2.757611	0.1591	LHEweight_wgt[481]	
0.5	-1.25	6.835341	0.5726	2.075247	0.1204	LHEweight_wgt[482]	
0.5	-1.0	5.030704	0.4273	1.491801	0.08696	LHEweight_wgt[483]	
0.5	-0.75	3.510528	0.2999	1.007273	0.05885	LHEweight_wgt[484]	
0.5	-0.5	2.274811	0.1982	0.621663	0.03658	LHEweight_wgt[485]	
0.5	-0.25	1.323555	0.1189	0.334972	0.01996	LHEweight_wgt[486]	
0.5	0.0	0.656969	0.06223	0.147253	0.008986	LHEweight_wgt[487]	
0.5	0.25	0.274423	0.02830	0.058342	0.003608	LHEweight_wgt[488]	
0.5	0.5	0.176548	0.01778	0.068404	0.003902	LHEweight_wgt[489]	
0.5	0.75	0.363132	0.03008	0.177385	0.009854	LHEweight_wgt[490]	
0.5	1.0	0.834177	0.06550	0.385283	0.02145	LHEweight_wgt[491]	
0.5	1.25	1.589682	0.1241	0.692099	0.03848	LHEweight_wgt[492]	
0.5	1.5	2.629647	0.2047	1.097834	0.06136	LHEweight_wgt[493]	
0.5	2.0	5.562958	0.4358	2.206057	0.1246	LHEweight_wgt[494]	
0.5	3.0	14.843102	1.177	5.609519	0.3172	LHEweight_wgt[495]	

**Table 4.2:**  $\kappa_V$  and  $\kappa_t$  combinations generated for the two signal samples and their NLO cross sections. The  $tHq$  cross section is multiplied by the branching fraction of the enforced leptonic decay of the top quark (0.324). See also Ref. [49].

Sample	$\sigma$ [pb]
TTWJetsToLNu_TuneCUETP8M1_13TeV-amcatnloFXFX-madspin-pythia8	0.2043
TTZToLLNuNu_M-10_TuneCUETP8M1_13TeV-amcatnlo-pythia8	0.2529
ttHJetToNonbb_M125_13TeV_amcatnloFXFX_madspin_pythia8_mWCutfix /store/cmst3/group/susy/gpetrucc/13TeV/u/TTLL_m1to10_LO_NoMS_for76X/	0.2151 0.0283
WGToLNuG_TuneCUETP8M1_13TeV-madgraphMLM-pythia8	585.8
ZGTo2LG_TuneCUETP8M1_13TeV-amcatnloFXFX-pythia8	131.3
TGJets_TuneCUETP8M1_13TeV_amcatnlo_madspin_pythia8	2.967
TGJets_TuneCUETP8M1_13TeV_amcatnlo_madspin_pythia8	2.967
TTGJets_TuneCUETP8M1_13TeV-amcatnloFXFX-madspin-pythia8	3.697
WpWpJJ_EWK-QCD_TuneCUETP8M1_13TeV-madgraph-pythia8	0.03711
ZZZ_TuneCUETP8M1_13TeV-amcatnlo-pythia8	0.01398
WWZ_TuneCUETP8M1_13TeV-amcatnlo-pythia8	0.1651
WZZ_TuneCUETP8M1_13TeV-amcatnlo-pythia8	0.05565
WW_DoubleScattering_13TeV-pythia8	1.64
tZq_ll_4f_13TeV-amcatnlo-pythia8_TuneCUETP8M1	0.0758
ST_tWll_5f_LO_13TeV-MadGraph-pythia8	0.01123
TTTT_TuneCUETP8M1_13TeV-amcatnlo-pythia8	0.009103
WZTo3LNu_TuneCUETP8M1_13TeV-powheg-pythia8	4.4296
ZZTo4L_13TeV_powheg_pythia8	1.256
TTJets_SingleLeptFromTbar_TuneCUETP8M1_13TeV-madgraphMLM-pythia8	182.1754
TTJets_SingleLeptFromT_TuneCUETP8M1_13TeV-madgraphMLM-pythia8	182.1754
TTJets_DiLept_TuneCUETP8M1_13TeV-madgraphMLM-pythia8	87.3
DYJetsToLL_M-10to50_TuneCUETP8M1_13TeV-amcatnloFXFX-pythia8	18610
DYJetsToLL_M-50_TuneCUETP8M1_13TeV-madgraphMLM-pythia8	6024
WJetsToLNu_TuneCUETP8M1_13TeV-amcatnloFXFX-pythia8	61526.7
ST_tW_top_5f_inclusiveDecays_13TeV-powheg-pythia8_TuneCUETP8M1	35.6
ST_tW_antitop_5f_inclusiveDecays_13TeV-powheg-pythia8_TuneCUETP8M1	35.6
ST_t-channel_4f_leptonDecays_13TeV-amcatnlo-pythia8_TuneCUETP8M1	70.3144
ST_t-channel_antitop_4f_leptonDecays_13TeV-powheg-pythia8_TuneCUETP8M1	26.2278
ST_s-channel_4f_leptonDecays_13TeV-amcatnlo-pythia8_TuneCUETP8M1	3.68064
WWTo2L2Nu_13TeV-powheg	10.481

**Table 4.3:** List of background samples used in this analysis (CMSSW 80X). In the first section of the table are listed the samples of the processes for which we use the simulation to extract the final yields and shapes, in the second section the samples of the processes we will estimate from data. The MC simulation is used to design the data driven methods and derive the associated systematics.

Sample	$\sigma$ [pb]
ttWJets_13TeV_madgraphMLM	0.6105
ttZJets_13TeV_madgraphMLM	0.5297/0.692

**Table 4.4:** Leading-order  $t\bar{t}W$  and  $t\bar{t}Z$  samples used in the signal BDT training.

Three lepton and Four lepton
HLT_DiMu9_Ele9_CaloIdL_TrackIdL_v*
HLT_Mu8_DiEle12_CaloIdL_TrackIdL_v*
HLT_TripleMu_12_10_5_v*
HLT_Ele16_Ele12_Ele8_CaloIdL_TrackIdL_v*
HLT_Mu23_TrkIsoVVL_Ele8_CaloIdL_TrackIdL_IsoVL_v*
HLT_Mu23_TrkIsoVVL_Ele8_CaloIdL_TrackIdL_IsoVL_DZ_v*
HLT_Mu8_TrkIsoVVL_Ele23_CaloIdL_TrackIdL_IsoVL_v*
HLT_Mu8_TrkIsoVVL_Ele23_CaloIdL_TrackIdL_IsoVL_DZ_v*
HLT_Ele23_Ele12_CaloIdL_TrackIdL_IsoVL_DZ_v*
HLT_Mu17_TrkIsoVVL_Mu8_TrkIsoVVL_DZ_v*
HLT_Mu17_TrkIsoVVL_TkMu8_TrkIsoVVL_DZ_v*
HLT_IsoMu22_v*
HLT_IsoTkMu22_v*
HLT_IsoMu22_eta2p1_v*
HLT_IsoTkMu22_eta2p1_v*
HLT_IsoMu24_v*
HLT_IsoTkMu24_v*
HLT_Ele27_WPTight_Gsf_v*
HLT_Ele25_eta2p1_WPTight_Gsf_v*
HLT_Ele27_eta2p1_WPLoose_Gsf_v*

**Table 4.5:** Table of high-level triggers that we consider in the analysis.

### 867 4.2.2 Triggers

868 We consider online-reconstructed events triggered by one, two, or three leptons.  
 869 Single-lepton triggers are included to boost the acceptance of events where the  $p_T$  of  
 870 the sub-leading lepton falls below the threshold of the double-lepton triggers. Ad-  
 871 ditionally, by including double-lepton triggers in the  $\geq 3$  lepton category, as well  
 872 as single-lepton triggers in all categories, we increase the efficiency, considering the  
 873 logical “or” of the trigger decisions of all the individual triggers in a given category.  
 874 Tab. 4.5 shows the lowest-threshold non-prescaled triggers present in the High-Level  
 875 Trigger (HLT) menus for both Monte-Carlo and data in 2016.

#### 876 4.2.2.1 Trigger efficiency scale factors

877 The efficiency of events to pass the trigger is measured in simulation (trivially using  
 878 generator information) and in the data (using event collected by an uncorrelated

Category	Scale Factor
ee	$1.01 \pm 0.02$
e $\mu$	$1.01 \pm 0.01$
$\mu\mu$	$1.00 \pm 0.01$
3l	$1.00 \pm 0.03$

**Table 4.6:** Trigger efficiency scale factors and associated uncertainties, shown here rounded to the nearest percent.

879 MET trigger). Small differences between the data and MC efficiencies are corrected  
 880 by applying scale factors as shown in Tab. 4.6. The exact procedure and control plots  
 881 are documented in [50] for the current analysis.

## 882 4.3 Object Identification and event selection

### 883 4.3.1 Jets and $b$ tagging

884 The analysis uses anti- $k_t$  (0.4) particle-flow (PF) jets, corrected for charged hadrons  
 885 not coming from the primary vertex (charged hadron subtraction), and having jet  
 886 energy corrections (`Summer16_23Sep2016V3`) applied as a function of the jet  $E_T$  and  
 887  $\eta$ . Jets are only considered if they have a transverse energy above 25GeV.

888 In addition, they are required to be separated from any lepton candidates passing  
 889 the fakeable object selections (see Tables 4.7 and 4.8) by  $\Delta R > 0.4$ .

890 The loose and medium working points of the CSV b-tagging algorithm are used to  
 891 identify  $b$  jets. Data/simulation differences in the  $b$  tagging performance are corrected  
 892 by applying per-jet weights to the simulation, dependent on the jet  $p_T$ , eta,  $b$  tagging  
 893 discriminator, and flavor (from simulation truth) [51]. The per-event weight is taken  
 894 as the product of the per-jet weights, including those of the jets associated to the  
 895 leptons. More details can be found in the corresponding  $t\bar{t}H$  documentation [47, 50].

896 **4.3.2 Lepton selection**

Cut	Loose	Fakeable object	Tight
$ \eta  < 2.4$	✓	✓	✓
$p_T$	$> 5\text{GeV}$	$> 15\text{GeV}$	$> 15\text{GeV}$
$ d_{xy}  < 0.05 \text{ (cm)}$	✓	✓	✓
$ d_z  < 0.1 \text{ (cm)}$	✓	✓	✓
$\text{SIP}_{3D} < 8$	✓	✓	✓
$I_{\text{mini}} < 0.4$	✓	✓	✓
is Loose Muon	✓	✓	✓
jet CSV	—	$< 0.8484$	$< 0.8484$
is Medium Muon	—	—	✓
tight-charge	—	—	✓
lepMVA $> 0.90$	—	—	✓

**Table 4.7:** Requirements on each of the three muon selections. In the cases where the cut values change between the selections, those values are listed in the table. Otherwise, whether the cut is applied is indicated. For the two  $p_T^{\text{ratio}}$  and CSV rows, the cuts marked with a † are applied to leptons that fail the lepton MVA cut, while the loose cut value is applied to those that pass the lepton MVA cut.

897       The lepton reconstruction and selection is identical to that used in the  $t\bar{t}H$  mul-  
 898 tilepton analysis, as documented in Refs. [47, 50]. For details on the reconstruction  
 899 algorithms, isolation, pileup mitigation, and a description of the lepton MVA discrim-  
 900 inator and validation plots thereof, we refer to that document since they are out of  
 901 the scope of this thesis. Three different selections are defined both for the electron  
 902 and muon object identification: the *Loose*, *Fakeable Object*, and *Tight* selection. As  
 903 described in more detail later, these are used for event level vetoes, the fake rate  
 904 estimation application region, and the final signal selection, respectively. The  $p_T$  of  
 905 fakeable objects is defined as  $0.85 \times p_T(\text{jet})$ , where the jet is the one associated to the  
 906 lepton object. This mitigates the dependence of the fake rate on the momentum of  
 907 the fakeable object and thereby improves the precision of the method.

908       Tables 4.7 and 4.8 list the full criteria for the different selections of muons and  
 909 electrons.

Cut	Loose	Fakeable Object	Tight
$ \eta  < 2.5$	✓	✓	✓
$p_T$	$> 7\text{GeV}$	$> 15\text{GeV}$	$> 15\text{GeV}$
$ d_{xy}  < 0.05 \text{ (cm)}$	✓	✓	✓
$ d_z  < 0.1 \text{ (cm)}$	✓	✓	✓
$\text{SIP}_{3D} < 8$	✓	✓	✓
$I_{\text{mini}} < 0.4$	✓	✓	✓
MVA ID $> (0.0, 0.0, 0.7)$	✓	✓	✓
$\sigma_{i\eta i\eta} < (0.011, 0.011, 0.030)$	—	✓	✓
$\text{H/E} < (0.10, 0.10, 0.07)$	—	✓	✓
$\Delta\eta_{in} < (0.01, 0.01, 0.008)$	—	✓	✓
$\Delta\phi_{in} < (0.04, 0.04, 0.07)$	—	✓	✓
$-0.05 < 1/E - 1/p < (0.010, 0.010, 0.005)$	—	✓	✓
$p_T^{\text{ratio}}$	—	$> 0.5 \dagger / -$	—
jet CSV	—	$< 0.3 \dagger / < 0.8484$	$< 0.8484$
tight-charge	—	—	✓
conversion rejection	—	—	✓
Number of missing hits	$< 2$	$== 0$	$== 0$
lepMVA $> 0.90$	—	—	✓

**Table 4.8:** Criteria for each of the three electron selections. In cases where the cut values change between selections, those values are listed in the table. Otherwise, whether the cut is applied is indicated. In some cases, the cut values change for different  $\eta$  ranges. These ranges are  $0 < |\eta| < 0.8$ ,  $0.8 < |\eta| < 1.479$ , and  $1.479 < |\eta| < 2.5$  and the respective cut values are given in the form (value<sub>1</sub>, value<sub>2</sub>, value<sub>3</sub>).

### 4.3.3 Lepton selection efficiency

Efficiencies of reconstruction and selecting loose leptons are measured both for muons and electrons using a tag and probe method on both data and MC, using  $Z \rightarrow \ell^+ \ell^-$ . Corresponding scale factors are derived from the ratio of efficiencies and applied to the selected These. Events are produced for the leptonic SUSY analyses using equivalent lepton selections and recycled for the  $t\bar{t}H$  analysis as well as for this analysis. The efficiencies of applying the tight selection as defined in Tables 4.7 and 4.8, on the loose leptons are determined again by using a tag and probe method on a sample of DY-enriched events. They are documented for the  $t\bar{t}H$  analysis in Ref. [50] and are exactly equivalent for this analysis.

## 920 4.4 Background predictions

921 The modeling of reducible and irreducible backgrounds in this analysis uses the exact  
 922 methods, analysis code, and ROOT trees used for the  $t\bar{t}H$  multilepton analysis. We  
 923 give a brief description of the methods and refer to the documentation of that analysis  
 924 in Refs. [47, 50] for any details.

925 The backgrounds in three-lepton final states can be split in two broad categories:  
 926 irreducible backgrounds with genuine prompt leptons (i.e. from on-shell W and Z  
 927 boson decays); and reducible backgrounds where at least one of the leptons is “non-  
 928 prompt”, i.e. produced within a hadronic jet, either a genuine lepton from heavy  
 929 flavor decays, or simply mis-reconstructed jets.

930 Irreducible backgrounds can be reliably estimated directly from Monte-Carlo sim-  
 931 ulated events, using higher-order cross sections or data control regions for the overall  
 932 normalization. This is done in this analysis for all backgrounds involving prompt lep-  
 933 tons:  $t\bar{t}W$ ,  $t\bar{t}Z$ ,  $t\bar{t}H$ ,  $WZ$ ,  $ZZ$ ,  $W^\pm W^\pm qq$ ,  $t\bar{t}t\bar{t}$ ,  $tZq$ ,  $tZW$ ,  $WWW$ ,  $WWZ$ ,  $WZZ$ ,  
 934  $ZZZ$ .

935 Reducible backgrounds, on the other hand, are not well predicted by simulation,  
 936 and are estimated using data-driven methods. In the case of non-prompt leptons, a  
 937 fake rate method is used, where the contribution to the final selection is estimated by  
 938 extrapolating from a sideband (or “application region”) with a looser lepton definition  
 939 (the fakeable object definitions in Tabs. 4.7 and 4.8) to the signal selection. The tight-  
 940 to-loose ratios (or “fake rates”) are measured in several background dominated data  
 941 events with dedicated triggers, subtracting the residual prompt lepton contribution  
 942 using MC. Non-prompt leptons in our signal regions are predominantly produced in  $t\bar{t}$   
 943 events, with a much smaller contribution, from Drell–Yan production. The systematic  
 944 uncertainty on the normalization of the non-prompt background estimation is on the

order of 50%, and thereby one of the dominant limitations on the performance of multilepton analyses in general and this analysis in particular. It consists of several individual sources, such as the result of closure tests of the method using simulated events, limited statistics in the data control regions due to necessary prescaling of lepton triggers, and the uncertainty in the subtraction of residual prompt leptons from the control region.

The fake background where the leptons pass the looser selection are weighted according to how many of them fail the tight criteria. Events with a single failing lepton are weighted with the factor  $f/(1-f)$  for the estimate to the tight selection region, where  $f$  is the fake rate. Events with two failing leptons are given the negative weight  $-f_i f_j / (1-f_i)(1-f_j)$ , and for three leptons the weight is positive and equal to the product of  $f/(1-f)$  factor evaluated for each failing lepton.

Figures 4.2 show the distributions of some relevant kinematic variables, normalized to the cross section of the respective processes and to the integrated luminosity.

## 4.5 Signal discrimination

The  $tHq$  signal is separated from the main backgrounds using a boosted decision tree (BDT) classifier, trained on simulated signal and background events. A set of discriminating variables are given as input to the BDT which produces a output distribution maximizing the discrimination power. Table 4.9 lists the input variables used while Figures 4.3 show their distributions for the relevant signal and background samples, for the three lepton channel. Two BDT classifiers are trained for the two main backgrounds expected in the analysis: events with prompt leptons from  $t\bar{t}W$  and  $t\bar{t}Z$ (also referred to as  $t\bar{t}V$ ), and events with non-prompt leptons from  $t\bar{t}$ . The datasets used in the training are the  $tHq$  signal (see Tab. 4.1), and LO MADGRAPH samples

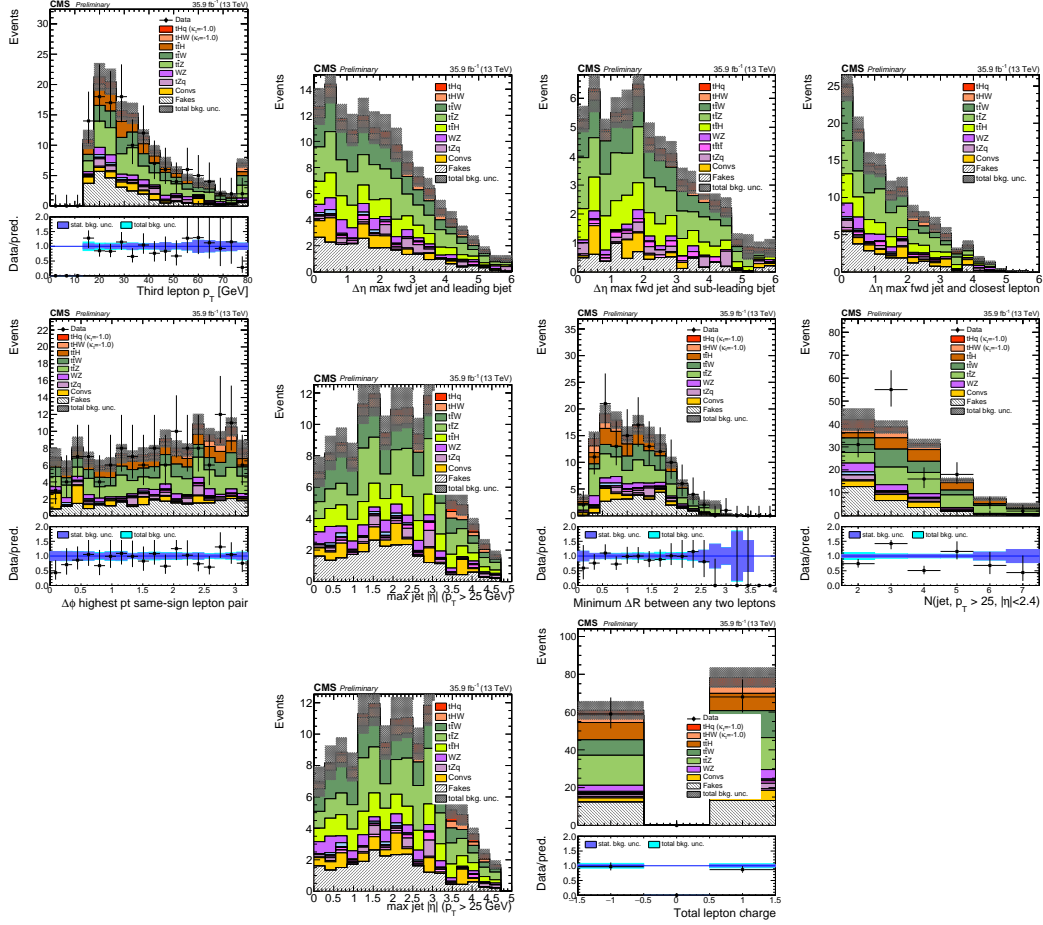


**Figure 4.2:** Distributions of input variables to the BDT for signal discrimination, three lepton channel, normalized to their cross section and to  $35.9\text{fb}^{-1}$ .

969 of  $t\bar{t}W$  and  $t\bar{t}Z$ , in an admixture proportional to their respective cross sections (see  
970 Tab. 4.4).

971 The MVA analysis consist of two stages: first a “training” where the MVA method  
972 is trained to discriminate between simulated signal and background events, then a  
973 “test” stage where the trained algorithm is used to classify different events from  
974 the samples. The sample is obtained from a pre-selection (see Tab. ?? with pre-  
975 selection cuts). Figures 4.4 show the input variables distributions as seen by the  
976 MVA algorithm. Note that in contrast to the distributions in Fig. 4.3 only the main  
977 backgrounds ( $t\bar{t}$  from simulation,  $t\bar{t}V$ ) are included.

Variable name	Description
nJet25	Number of jets with $p_T > 25$ GeV, $ \eta  < 2.4$
MaxEtaJet25	Maximum $ \eta $ of any (non-CSV-loose) jet with $p_T > 25$ GeV
totCharge	Sum of lepton charges
nJetEta1	Number of jets with $ \eta  > 1.0$ , non-CSV-loose
detaFwdJetBJet	$\Delta\eta$ between forward light jet and hardest CSV loose jet
detaFwdJet2BJet	$\Delta\eta$ between forward light jet and second hardest CSV loose jet (defaults to -1 in events with only one CSV loose jet)
detaFwdJetClosestLep	$\Delta\eta$ between forward light jet and closest lepton
dphiHighestPtSSPair	$\Delta\phi$ of highest $p_T$ same-sign lepton pair
minDRll	minimum $\Delta R$ between any two leptons
Lep3Pt/Lep2Pt	$p_T$ of the 3 <sup>rd</sup> lepton (2 <sup>nd</sup> for ss2l)

**Table 4.9:** MVA input discriminating variables

978 Note that splitting the training in two groups reveals that some variables show  
 979 opposite behavior for the two background sources; potentially screening the discrimi-  
 980 nation power if they were to be used in a single discriminant. For some other variables  
 981 the distributions are similar in both background cases.

982 From table 4.9, it is clear that the input variables are correlated to some extend.  
 983 These correlations play an important role for some MVA methods like the Fisher  
 984 discriminant method in which the first step consist of performing a linear transfor-  
 985 mation to an phase space where the correlations between variables are removed. In  
 986 case a boosted decision tree (BDT) method however, correlations do not affect the  
 987 performance. Figure 4.6 show the linear correlation coefficients for signal and back-  
 988 ground for the two training cases (the signal values are identical by construction). As  
 989 expected, strong correlations appears for variables related to the forward jet activity.  
 990 Same trend is seen in case of the same sign dilepton channel in Figure ??.

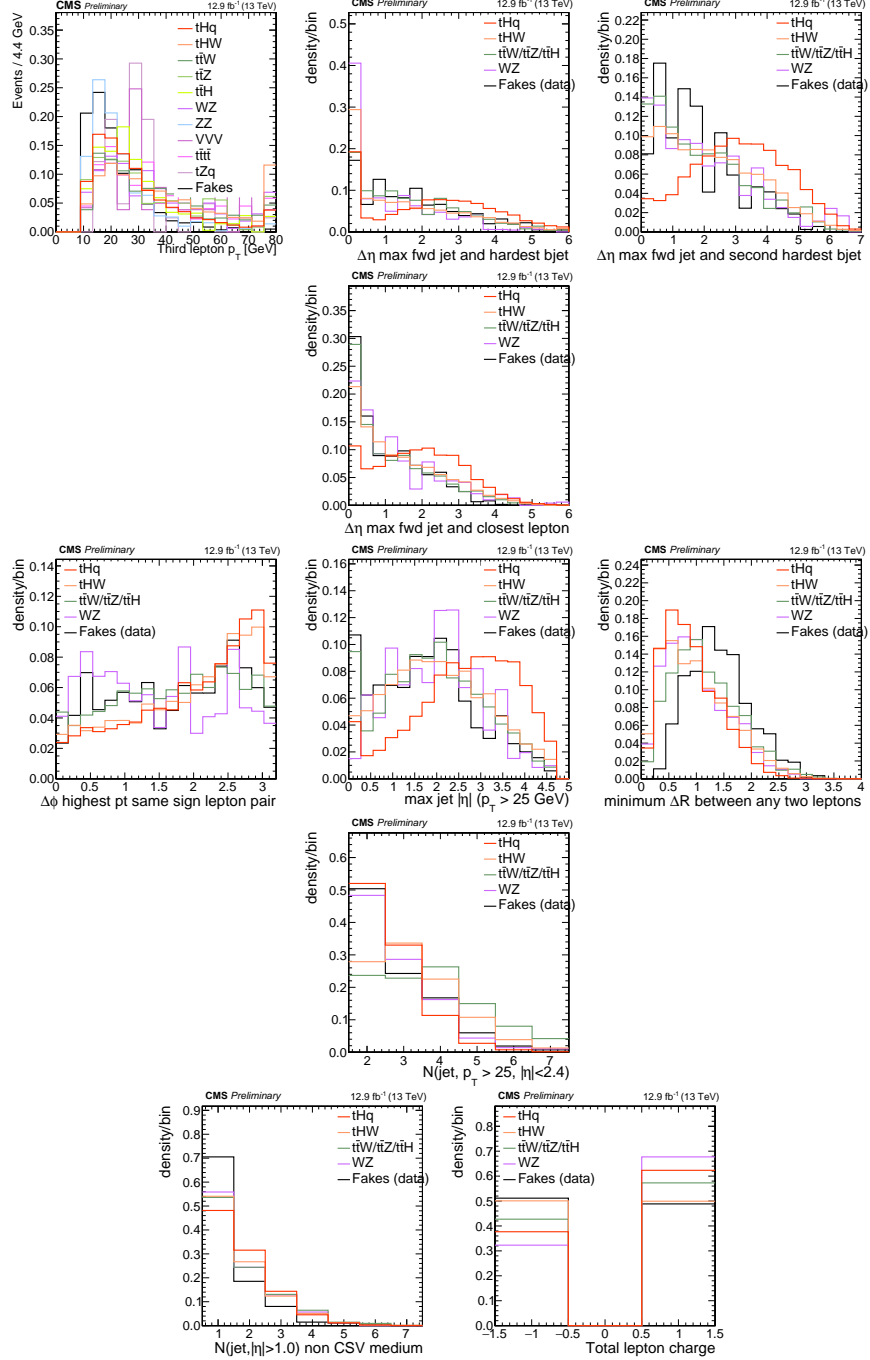


**Figure 4.3:** Distributions of input variables to the BDT for signal discrimination, three lepton channel.

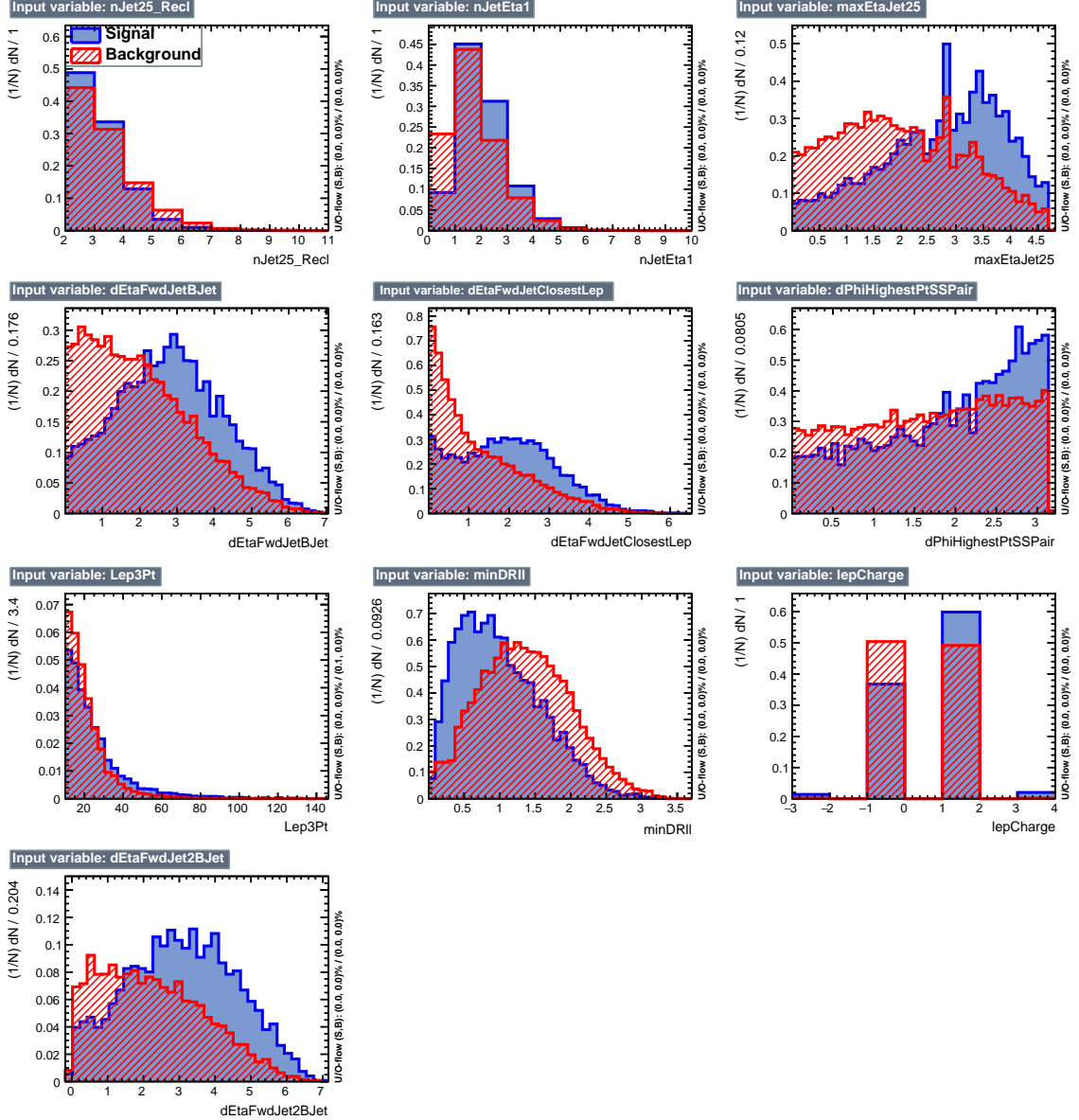


**Figure 4.4:** BDT inputs as seen by TMVA (signal, in blue, is  $tHq$ , background, in red, is  $t\bar{t}$ ) for the three lepton channel, discriminated against  $t\bar{t}$  (fakes) background.

### 991 4.5.1 Classifiers response

992 Several MVA algorithms were evaluated to determine the most appropriate method  
 993 for this analysis. The plots in Fig. 4.7 (top) show the background rejection as a  
 994 function of the signal efficiency for  $t\bar{t}$  and  $t\bar{t}V$  trainings (ROC curves) for the different

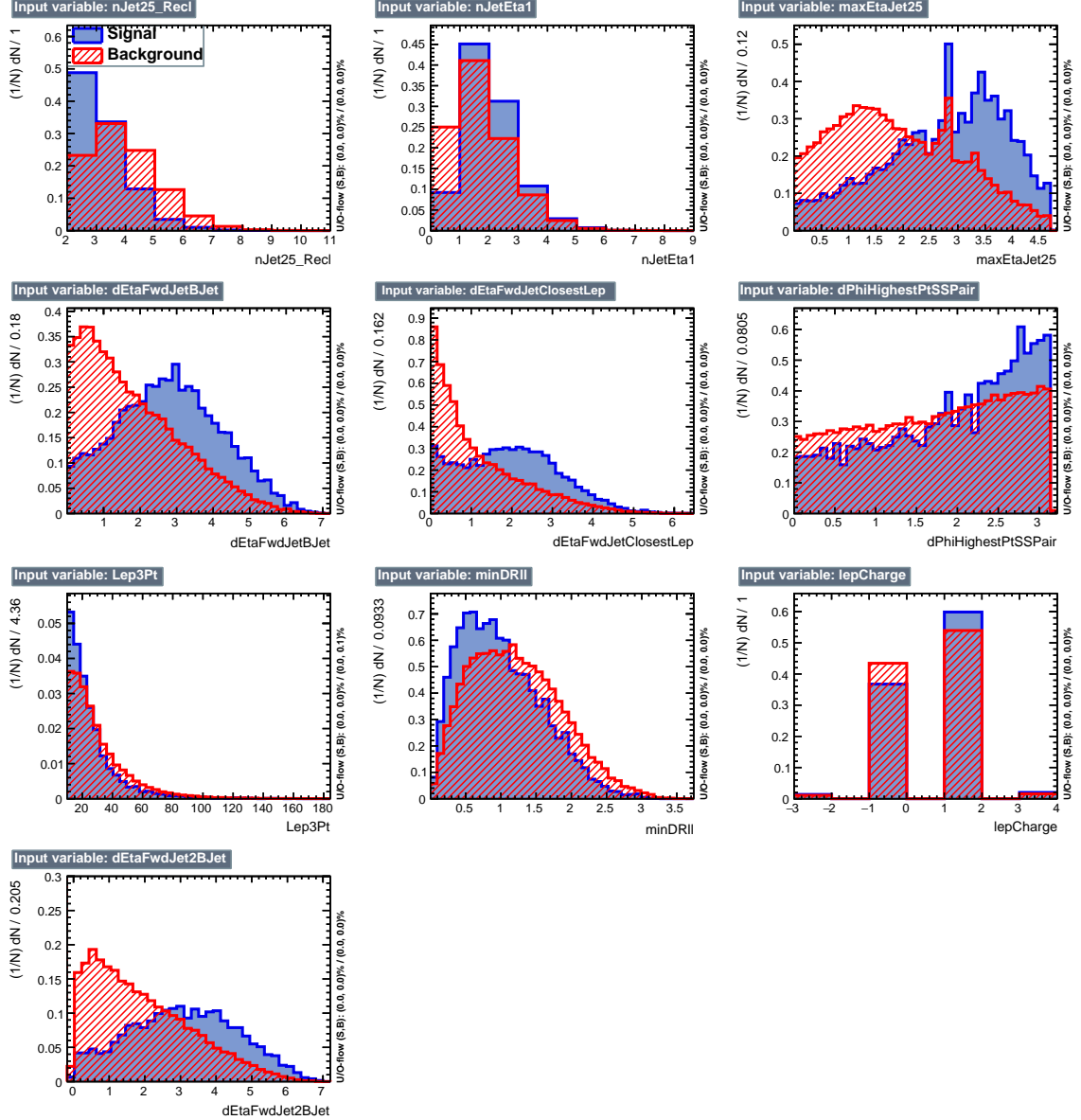


**Figure 4.5:** BDT inputs as seen by TMVA (signal, in blue, is  $tHq$ , background, in red, is  $t\bar{t}W+t\bar{t}Z$ ) for the three lepton channel, discriminated against  $t\bar{t}V$  background.

algorithms that were evaluated.

In both cases the gradient boosted decision tree (“BDTA\_GRAD”) classifier offers the best results, followed by an adaptive BDT classifier (“BDTA”). The BDTA\_GRAD classifier output distributions for signal and backgrounds are shown on the bottom of Fig. 4.7. As expected, a good discrimination power is obtained using default discrim-

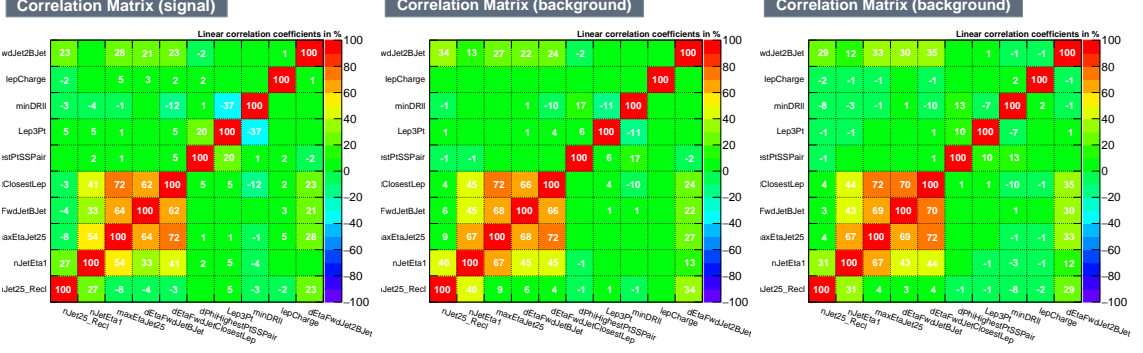


**Figure 4.6:** Signal (left),  $t\bar{t}$  background (middle), and  $t\bar{t}V$  background (right.) correlation matrices for the input variables in the TMVA analysis for the three lepton channel.

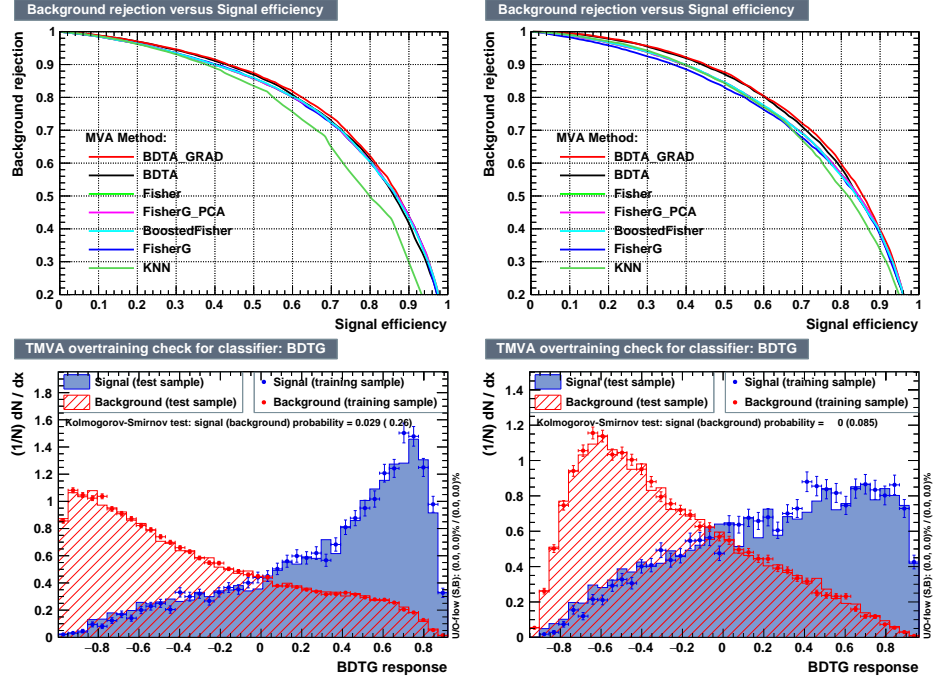


**Figure 4.7:** Top: background rejection vs signal efficiency (ROC curves) for various MVA classifiers (top) in the three lepton channel against  $t\bar{t}V$  (left) and  $t\bar{t}$  (right). Bottom: classifier output distributions for the gradient boosted decision trees, for training against  $t\bar{t}V$  (left) and against  $t\bar{t}$  (right).

1000 inator parameter values, with minimal overtraining. TMVA provides a ranking of the  
 1001 input variables by their importance in the classification process, shown in Tab. 4.10.  
 1002 The TMVA settings used in the BDT training are shown in Tab. 4.11.

ttbar training			ttV training		
Rank	Variable	Importance	Variable	Importance	
1	minDRll	1.329e-01	dEtaFwdJetBJet	1.264e-01	
2	dEtaFwdJetClosestLep	1.294e-01	Lep3Pt	1.224e-01	
3	dEtaFwdJetBJet	1.209e-01	maxEtaJet25	1.221e-01	
4	dPhiHighestPtSSPair	1.192e-01	dEtaFwdJet2BJet	1.204e-01	
5	Lep3Pt	1.158e-01	dEtaFwdJetClosestLep	1.177e-01	
6	maxEtaJet25	1.121e-01	minDRll	1.143e-01	
7	dEtaFwdJet2BJet	9.363e-02	dPhiHighestPtSSPair	9.777e-02	
8	nJetEta1	6.730e-02	nJet25_Recl	9.034e-02	
9	nJet25_Recl	6.178e-02	nJetEta1	4.749e-02	
10	lepCharge	4.701e-02	lepCharge	4.116e-02	

**Table 4.10:** TMVA input variables ranking for BDTA\_GRAD method for the trainings in the three lepton channel. For both trainings the rankings show almost the same 5 variables in the first places.

---

```
TMVA.Types.kBDT
NTrees=800
BoostType=Grad
Shrinkage=0.10
!UseBaggedGrad
nCuts=50
MaxDepth=3
NegWeightTreatment=PairNegWeightsGlobal
CreateMVApdfs
```

---

**Table 4.11:** TMVA configuration used in the BDT training.

## 1003 4.6 Additional discriminating variables

1004 Two additional discriminating variables were tested considering the fact that the  
 1005 forward jet in the background could come from the pileup; since we have a real  
 1006 forward jet in the signal, it could give some improvement in the discriminating power.  
 1007 The additional variables describe the forward jet momentum (fwdJetPt25) and the  
 1008 forward jet identification(fwdJetPUID). Distributions for these variables in the three  
 1009 lepton channel are shown in the figure 4.8. The forward jet identification distribution  
 1010 show that for both, signal and background, jets are mostly real jets.

1011 The testing was made including in the MVA input one variable at a time, so we

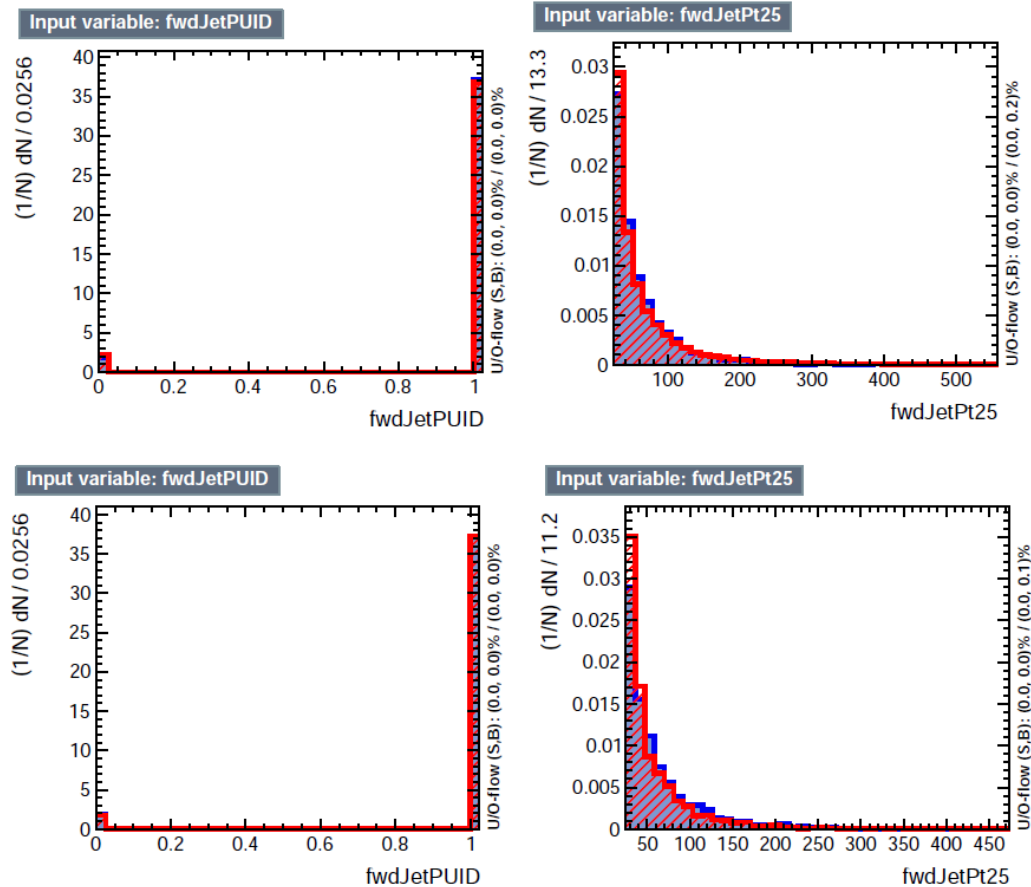


**Figure 4.8:** Additional discriminating variables distributions for ttV training (Top row) and tt training (bottom row) in the three lepton channel. The origin of the jets in the forward jet identification distribution is tagged as 0 for “pileup jets” while “real jets” are tagged as 1.

1012 can evaluate the discrimination power of each variable, and then both simultaneously.  
 1013 fwdJetPUID was ranked in the last place in importance (11) in both training (ttV  
 1014 and tt) while fwdJetPt25 was ranked 3 in the ttV training and 7 in the tt training.  
 1015 When training using 12 variables, fwdJetPt25 was ranked 5 and 7 in the ttV and tt  
 1016 trainings respectively, while fwdJetPUID was ranked 12 in both cases.

1017 The improvement in the discrimination performance provided by the additional  
 1018 variables is about 1%, so it was decided not to include them in the procedure. Table  
 1019 4.12 show the ROC-integral for all the testing cases we made.

ROC-integral	
base 10 var ttv	0.848
+ fwdJetPUID ttv	0.849
+ fwdJetPt25 ttv	0.856
12 var ttv	0.856
<hr/>	
base 10 var tt	0.777
+ fwdJetPUID tt	0.777
+ fwdJetPt25 tt	0.787
12 var	0.787

**Table 4.12:** ROC-integral for all the testing cases we made in the evaluation of the additional variables discriminating power. The improvement in the discrimination performance provided by the additional variables is about 1%

1020 **Chapter 5**

1021 **The CMS forward pixel detector**

1022 **5.0.1 The phase 1 FPix upgrade**

1023 **5.0.2 FPix module production line**

1024 **5.0.3 The Gluing stage**

1025 **5.0.4 The Encapsulation stage**

1026 **5.0.5 The FPix module production yields**

<sup>1027</sup> **References**

- <sup>1028</sup> [1] D.J. Griffiths, “Introduction to electrodynamics”. 4th ed. Pearson, (2013).
- <sup>1029</sup> [2] F. Mandl, G. Shaw. “Quantum field theory.” Chichester: Wiley (2009).
- <sup>1030</sup> [3] F. Halzen, and A.D. Martin, “Quarks and leptons: An introductory course in  
<sup>1031</sup> modern particle physics”. New York: Wiley, (1984) .
- <sup>1032</sup> [4] J.C. Maxwell. “A dynamical theory of the electromagnetic field”. Philosophical  
<sup>1033</sup> Transactions of the Royal Society of London. 155: 459–512.(1865)  
<sup>1034</sup> doi:10.1098/rstl.1865.0008
- <sup>1035</sup> [5] M. Planck. “Über das Gesetz der Energieverteilung im Normalspektrum”.  
<sup>1036</sup> Annalen der Physik. 4 (3): 553.(1901).
- <sup>1037</sup> [6] A. Einstein “Über einen die Erzeugung und Verwandlung des Lichtes betref-  
<sup>1038</sup> fenden heuristischen Gesichtspunkt”. Annalen der Physik. 17 (6): 132–148,  
<sup>1039</sup> (1905).
- <sup>1040</sup> [7] A. Einstein. “Über die von der molekularkinetischen Theorie der Wärme  
<sup>1041</sup> geforderte Bewegung von in ruhenden Flüssigkeiten suspendierten Teilchen”.  
<sup>1042</sup> Annalen der Physik. 17 (8): 549–560, (1905).
- <sup>1043</sup> [8] A. Einstein. “Zur Elektrodynamik bewegter Körper”. Annalen der Physik. 17  
<sup>1044</sup> (10): 891–921, (1905).

- 1045 [9] A. Einstein, "Ist die TrÄdgheit eines KÃürpers von seinem Energieinhalt ab-  
 1046 hÃdngig?". Annalen der Physik. 18 (13): 639â€¢641, (1905).
- 1047 [10] B. P. Abbott et al. "Observation of Gravitational Waves from a Binary Black  
 1048 Hole Merger". PRL 116, 061102 (2016).
- 1049 [11] J. Schwinger. "Quantum Electrodynamics. I. A Covariant Formulation". Phys-  
 1050 ical Review. 74 (10): 1439â€¢61, (1948).
- 1051 [12] R. P. Feynman. "Spaceâ€¢Time Approach to Quantum Electrodynamics".  
 1052 Physical Review. 76 (6): 769â€¢89, (1949).
- 1053 [13] S. Tomonaga. "On a Relativistically Invariant Formulation of the Quantum  
 1054 Theory of Wave Fields". Progress of Theoretical Physics. 1 (2): 27â€¢42, (1946).
- 1055 [14] S.L. Glashow. "Partial symmetries of weak interactions", Nucl. Phys. 22 579-  
 1056 588, (1961).
- 1057 [15] A. Salam, J.C. Ward. "Electromagnetic and weak interactions", Physics Letters  
 1058 13 168-171, (1964).
- 1059 [16] S. Weinberg, "A model of leptons", Physical Review Letters, vol. 19, no. 21, p.  
 1060 1264, (1967).
- 1061 [17] E. Noether, "Invariante Variationsprobleme", Nachrichten von der Gesellschaft  
 1062 der Wissenschaften zu GÃüttingen, mathematisch-physikalische Klasse, vol.  
 1063 1918, pp. 235â€¢257, (1918).
- 1064 [18] File:Standard\_Model\_of\_Elementary\_Particle\_dark.svg. (2017, June 12)  
 1065 Wikimedia Commons, the free media repository. Retrieved November 27,  
 1066 2017 from <https://www.collegiate-advanced-electricity.com/single-post/2017/04/10/The-Standard-Model-of-Particle-Physics>.

- 1068 [19] M. Goldhaber, L. Grodzins, A.W. Sunyar “Helicity of Neutrinos”, Phys. Rev.  
 1069 109, 1015 (1958).
- 1070 [20] Palanque-Delabrouille N et al. “Neutrino masses and cosmology with Lyman-  
 1071 alpha forest power spectrum”, JCAP 11 011 (2015).
- 1072 [21] C. Patrignani et al. (Particle Data Group), Chin. Phys. C, 40, 100001 (2016)  
 1073 and 2017 update.
- 1074 [22] M. Gell-Mann. “A Schematic Model of Baryons and Mesons”. Physics Letters.  
 1075 8 (3): 214–215 (1964).
- 1076 [23] G. Zweig. “An SU(3) Model for Strong Interaction Symmetry and its Breaking”  
 1077 (PDF). CERN Report No.8182/TH.401 (1964).
- 1078 [24] G. Zweig. “An SU(3) Model for Strong Interaction Symmetry and its Breaking:  
 1079 II” (PDF). CERN Report No.8419/TH.412(1964).
- 1080 [25] M. Gell-Mann. “The Interpretation of the New Particles as Displaced Charged  
 1081 Multiplets”. Il Nuovo Cimento 4: 848. (1956).
- 1082 [26] T. Nakano, K. Nishijima. “Charge Independence for V-particles”. Progress of  
 1083 Theoretical Physics 10 (5): 581-582. (1953).
- 1084 [27] N. Cabibbo, “Unitary symmetry and leptonic decays” Physical Review Letters,  
 1085 vol. 10, no. 12, p. 531, (1963).
- 1086 [28] M.Kobayashi, T.Maskawa, “CP-violation in the renormalizable theory of weak  
 1087 interaction,” Progress of Theoretical Physics, vol. 49, no. 2, pp. 652-657, (1973).
- 1088 [29] File:Weak Decay (flipped).svg. (2017, June 12). Wikimedia Com-  
 1089 mons, the free media repository. Retrieved November 27, 2017

- 1090       from     `https : //commons.wikimedia.org/w/index.php?title = File :`  
 1091       `Weak_Decay_(flipped).svg&oldid = 247498592.`
- 1092 [30] Georgia Tech University. Coupling Constants for the Fundamental  
 1093 Forces(2005). Retrieved January 10, 2018, from `http://hyperphysics.phy –`  
 1094 `astr.gsu.edu/hbase/Forces/couple.html#c2`
- 1095 [31] M. Strassler. (May 31, 2013).The Strengths of the Known Forces. Retrieved  
 1096 January 10, 2018, from `https://profmattstrassler.com/articles – and –`  
 1097 `posts/particle – physics – basics/the – known – forces – of – nature/the –`  
 1098 `strength – of – the – known – forces/`
- 1099 [32] M. Peskin, D. Schroeder, “An introduction to quantum field theory”. Perseus  
 1100 Books Publishing L.L.C., (1995).
- 1101 [33] A. Pich. “The Standard Model of Electroweak Interactions”  
 1102 `https://arxiv.org/abs/1201.0537`
- 1103 [34] F.Bellaiche. (2012, 2 September). “What’s this Higgs boson anyway?”. Retrieved  
 1104 from: `https://www.quantum-bits.org/?p=233`
- 1105 [35] M. Endres et al. Nature 487, 454-458 (2012) doi:10.1038/nature11255
- 1106 [36] F. Englert, R. Brout. “Broken Symmetry and the Mass of Gauge Vec-  
 1107 tor Mesons”. Physical Review Letters. 13 (9): 321–323.(1964) Bib-  
 1108 code:1964PhRvL..13..321E. doi:10.1103/PhysRevLett.13.321
- 1109 [37] P.Higgs. “Broken Symmetries and the Masses of Gauge Bosons”. Physical  
 1110 Review Letters. 13 (16): 508–509,(1964). Bibcode:1964PhRvL..13..508H.  
 1111 doi:10.1103/PhysRevLett.13.508.

- 1112 [38] G.Guralnik, C.R. Hagen and T.W.B. Kibble. “Global Conservation Laws and  
 1113 Massless Particles”. Physical Review Letters. 13 (20): 585–587, (1964). Bib-  
 1114 code:1964PhRvL..13..585G. doi:10.1103/PhysRevLett.13.585.
- 1115 [39] CMS collaboration. “Observation of a new boson at a mass of 125  
 1116 GeV with the CMS experiment at the LHC”. Physics Letters B.  
 1117 716 (1): 30–61 (2012). arXiv:1207.7235. Bibcode:2012PhLB..716...30C.  
 1118 doi:10.1016/j.physletb.2012.08.021
- 1119 [40] ATLAS collaboration. “Observation of a New Particle in the Search for  
 1120 the Standard Model Higgs Boson with the ATLAS Detector at the LHC”.  
 1121 Physics Letters B. 716 (1): 1–29(2012). arXiv:1207.7214. Bib-  
 1122 code:2012PhLB..716....1A. doi:10.1016/j.physletb.2012.08.020.
- 1123 [41] ATLAS collaboration; CMS collaboration (26 March 2015). “Combined  
 1124 Measurement of the Higgs Boson Mass in pp Collisions at  $\sqrt{s}=7$  and  
 1125 8 TeV with the ATLAS and CMS Experiments”. Physical Review Let-  
 1126 ters. 114 (19): 191803. arXiv:1503.07589. Bibcode:2015PhRvL.114s1803A.  
 1127 doi:10.1103/PhysRevLett.114.191803.
- 1128 [42] CMS Collaboration, “SM Higgs Branching Ratios and To-  
 1129 tal Decay Widths (up-date in CERN Report4 2016)”.  
 1130 <https://twiki.cern.ch/twiki/bin/view/LHCPhysics/CERNYellowReportPageBR>  
 1131 , last accessed on 17.12.2017.
- 1132 [43] R.Grant V. “Determination of Higgs branching ratios in  $H \rightarrow W^+W^- \rightarrow l^+l^- jj$  and  $H \rightarrow ZZ \rightarrow l^+l^- jj$  channels”. Physics Department, Uni-  
 1133 versity of Tennessee (Dated: October 31, 2012). Retrieved from  
 1134 <http://aesop.phys.utk.edu/ph611/2012/projects/Riley.pdf>

- 1136 [44] LHC Higgs Cross Section Working Group, Denner, A., Heinemeyer, S. et al.  
 1137 “Standard model Higgs-boson branching ratios with uncertainties”. Eur. Phys.  
 1138 J. C (2011) 71: 1753. <https://doi.org/10.1140/epjc/s10052-011-1753-8>
- 1139 [45] CMS Collaboration, “Search for the associated production of a Higgs boson  
 1140 with a single top quark in proton-proton collisions at  $\sqrt{s} = 8$  TeV”, JHEP 06  
 1141 (2016) 177, doi:10.1007/JHEP06(2016)177, arXiv:1509.08159.
- 1142 [46] B. Stieger, C. Jorda Lope et al., “Search for Associated Production of a Single  
 1143 Top Quark and a Higgs Boson in Leptonic Channels”, CMS Analysis Note CMS  
 1144 AN-14-140, 2014.
- 1145 [47] M. Peruzzi, C. Mueller, B. Stieger et al., “Search for ttH in multilepton final  
 1146 states at  $\sqrt{s} = 13$  TeV”, CMS Analysis Note CMS AN-16-211, 2016.
- 1147 [48] CMS Collaboration, “Search for H to bbar in association with a single top quark  
 1148 as a test of Higgs boson couplings at  $\sqrt{s} = 13$  TeV”, CMS Physics Analysis  
 1149 Summary CMS-PAS-HIG-16-019, 2016.
- 1150 [49] B. Maier, “SingleTopHiggProduction13TeV”, February, 2016.  
 1151 <https://twiki.cern.ch/twiki/bin/viewauth/CMS/SingleTopHiggsGeneration13TeV>.
- 1152 [50] M. Peruzzi, F. Romeo, B. Stieger et al., “Search for ttH in multilepton final  
 1153 states at  $\sqrt{s} = 13$  TeV”, CMS Analysis Note CMS AN-17-029, 2017.
- 1154 [51] B. WG, “BtagRecommendation80XReReco”, February, 2017.  
 1155 <https://twiki.cern.ch/twiki/bin/view/CMS/BtagRecommendation80XReReco>.